OPTICAL LATTICES

P. S. JESSEN

Optical Sciences Center
University of Arizona
Tucson, AZ, 85721
Phone: (520) 621-8267
Fax: (520) 621-6778
e-mail: jessen@rhea.opt-sci.arizona.edu

I. H. DEUTSCH

Center for Advanced Studies
University of New Mexico
Albuquerque, NM, 87131
Phone: (505) 277-1502
Fax: (505) 277-1520
e-mail: ideutsch@tangelo.phys.unm.edu

To appear in *Advances in Atomic, Molecular and Optical Physics* ***37***, eds. B. Bederson and H. Walther. (Academic Press, Cambridge, 1996).

CONTENTS

I. Introduction.....3

II. The 1D lin⊥lin Model System.....4
A. Atomic Motion in a 1D lin⊥lin Optical Lattice.....4
B. Spectroscopy in 1D lin⊥lin Optical Lattices.....7

III. Crystallography of Optical Lattices.....10
A. Two Dimensional Lattices.....12
B. Three Dimensional Lattices.....14

IV. Laser Cooling In Optical Lattices: Theory.....14
A. General Formalism.....16
B. Semiclassical Methods.....18
C. The Monte-Carlo Wave Function Technique.....19
D. Band Structure Formalism.....20
E. The Secular Approximation.....23

V. Spectroscopy.....25
A. Spectroscopic Techniques.....26
B. Experimental Results.....29

IV. New Developments.....33
A. Cooling by Adiabatic Expansion in Optical Lattices.....33
B. Bragg Scattering in Optical Lattices.....35
C. Outlook.....38

I. Introduction

The interference pattern of a set of intersecting laser beams can create a stable periodic potential for neutral atoms through the AC Stark shift (light shift), which can trap, and thereby organize atoms in an ordered, crystal-like structure. Historically, interest in these "optical lattices" grew out of the study of laser cooling (Hänsch and Schawlow, 1975; Wineland and Dehmelt, 1975). In 1988 the group at NIST Gaithersburg (Lett et al., 1988) discovered that atoms are readily cooled below the so called "Doppler limit". Research at the Ecole Normale Supérieure (Dalibard and Cohen-Tannoudji, 1989) and Stanford (Ungar et al., 1989) soon thereafter identified new mechanisms for laser cooling that occur for atoms with degenerate ground states and light fields with spatially varying polarization. The ENS group in particular proposed an elegant 1-dimensional model system, in which cooling results from optical pumping between a set of spatially varying light shift potentials that depend on the atomic ground state. This model system cannot, however, be easily compared with the standard laser cooling configuration, known as optical *molasses*, which involves six laser beams and results in a complicated 3-dimensional laser field of spatio-temporally varying intensity and polarization. Considerable effort was therefore directed towards realizing the 1-dimensional model system in the laboratory. The first experiments of this type immediately lead to spectacular new physical insight, prominent examples of which are atom trapping in microscopic optical potential wells, quantized atomic center-of-mass motion, and the generation of atomic samples with long range order imposed by light fields. At this point the concept of an optical *lattice* was coined, signifying a shift away from a physical image of laser cooled atoms as a disordered vapor (optical molasses), towards a new physical image of an atomic sample whose properties are primarily determined by the periodic optical potential.

Aside from its role as a model system for laser cooling, the motion of atoms in an optical lattice is closely analogous to that of an electron in a solid state crystal. This situation offers unique opportunities to explore phenomena that were previously accessible only in condensed matter. In contrast to a solid, where the distance between atoms is a few angstroms, the inter-particle spacing in an optical lattice can be many micrometers. Thus, the system can be essentially free from strong atom-atom interactions, which are difficult to model analytically, and must be treated by approximate or numerical methods. Even at densities that are large by the standards of a typical laser cooling experiment, the inter-atomic interactions are sufficiently small that they can be studied using tractable, accurate theories. The optical lattice potential itself can be modeled exactly, and can be produced in the laboratory without defects if appropriate attention is given to laser beam quality. Parameters characterizing the lattice, such as lattice constants/symmetry, and potential well

depth/shape are easily adjusted through choices of the laser geometry, polarization, intensity, and frequency. Furthermore, the dissipative aspects of the dynamics, arising from spontaneous emission, is in principle controllable through adjustments of the laser frequency and intensity, and its description is within the range of an abinitio theory. These considerations suggest that the atom/lattice system provides an attractive combination of tractable theory and well-controlled experiments, and so may prove a valuable testing ground for new developments in condensed matter physics. Examples of problems that may be addressed range from quantum transport phenomena to the physics of systems that exhibit long-range, but not short-range, order.

In this chapter we will review the experimental and theoretical developments in the study of optical lattices. In sect. II we introduce our subject by discussing the key 1-dimensional model system for laser cooling and trapping in optical lattices. In sect. III we discuss crystallography of various lattice geometries, and in sect. IV we cover the basic laser cooling theory in optical lattices. Sect. V reviews experimental work that probes optical lattices through spectroscopy, and finally, in sect. VI we discuss new developments in the field and possible future directions.

II. The 1D lin⊥lin Model System

In this section we discuss a 1-dimensional (1D) model system identified by Dalibard and Cohen-Tannoudji (1989). This system consists of an atom with angular momenta $J_g = 1/2$ in the ground state and $J_e = 3/2$ in the excited state, moving in an optical lattice formed by a pair of linear and cross-polarized counter-propagating plane waves; in the following we refer to this configuration as "1D lin⊥lin". Our use of the term 1D refers to the single dimension along which the field polarization and/or intensity is varying. In the remaining two dimensions the atoms are neither trapped nor cooled; motion in this plane is, to a good approximation, not probed by experiments and therefore is ignored.

A. Atomic Motion in a 1D Lin⊥Lin Optical Lattice

Consider the 1D lin⊥lin optical lattice shown in Fig 1b, composed of two counterprogating plane waves with orthogonal, linear polarizations $\hat{\mathbf{x}}$ and $\hat{\mathbf{y}}$ traveling in the directions $\pm\hat{\mathbf{z}}$. The total electric field is $\mathbf{E}_L(z,t) = \frac{1}{2}\mathbf{E}_L(z)e^{-i\omega t} + c.c$, where the spatial part, by convenient choice of phase and quantization axis along $\hat{\mathbf{z}}$, can be written as

$$\mathbf{E}_L(z) = -E_0\left[\hat{\mathbf{x}}e^{ikz} + i\hat{\mathbf{y}}e^{-ikz}\right] = \sqrt{2}E_0\left[\hat{\mathbf{e}}_+\cos(kz) - i\hat{\mathbf{e}}_-\sin(kz)\right]. \tag{1}$$

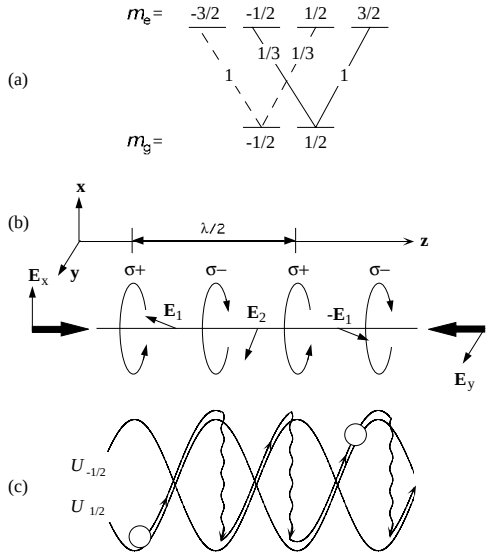

Fig. 1. Sisyphus cooling. (a) Level structure of a $J_g = 1/2 \rightarrow J_e = 3/2$ atom, including the square of the Clebsch-Gordan coefficients. (b) 1D lin⊥lin lattice configuration. (c) Example of a trajectory followed by an atom in the bipotential associated with the two ground state sublevels. Optical pumping predominantly transfers an atom from the hills of one optical potential to the valleys of the other, and the atom's kinetic energy is dissipated.

Equation (1) shows that the total field can be decomposed into two standing waves of σ_+ and σ_- polarization, offset by $\lambda/4$ so that the antinodes of one coincides with the nodes of the other. Note that the light intensity $I_L \propto |E_L(z)|^2$ is everywhere constant; only the field polarization changes from circular to linear and back to circular as one moves a distance $\lambda/4$ along $\hat{\mathbf{z}}$. Fig. 1a shows the level structure of an atom with ground and excited state angular momenta $J_g = 1/2$ and $J_e = 3/2$. Since the electric field contains only $\sigma_\pm$ components, the atom-laser interaction consists of two independent "V-systems", $\{|e,-1/2\rangle, |g,1/2\rangle, |e,3/2\rangle\}$ and $\{|e,-3/2\rangle, |g,-1/2\rangle, |e,1/2\rangle\}$, coupled only through $\Delta m = 0$ spontaneous decay of the $|e,\pm 1/2\rangle$ states. In the limit of low saturation, the optical potentials for the $|g,\pm 1/2\rangle$ states are (Dalibard and Cohen-Tannoudji, 1989),

$$U_{1/2}(z) = \frac{2}{3}U_0 \cos^2(kz) + \frac{1}{3}U_0 \quad , \quad U_{-1/2}(z) = \frac{2}{3}U_0 \sin^2(kz) + \frac{1}{3}U_0, \tag{2}$$

where $U_0 = \hbar \Delta s_0 / 2$ is the maximum value of the light shift (negative for $\Delta<0$). In these expressions $s_0 = 2\Omega^2 / \left(4\Delta^2 + \Gamma^2\right)$ is the saturation parameter for the $|g,1/2\rangle \leftrightarrow |e,3/2\rangle$

transition at a point where the polarization is purely σ_+, with associated Rabi frequency Ω, and detuning $\Delta = \omega_A - \omega_L$ of the lattice light from atomic resonance.In a red detuned lattice, $\Delta<0$, laser cooling occurs because of optical pumping between the atomic ground state sublevels. In the following we regard the center-of-mass position and momentum of the atom as classical variables in order to visualize how kinetic energy is dissipated. Consider an atom moving along $\hat{\mathbf{z}}$ as illustrated in Fig. 1c. At some time the atom is in the state $|g,1/2\rangle$ at an antinode of the σ_+ standing wave. This corresponds to a location at the bottom of a well in the potential $U_{1/2}$. As the atom moves away from the σ_+ antinode it expends kinetic energy by climbing out of the $U_{1/2}$ potential well. At first it is unlikely that the atom will optically pump to the state $|g,-1/2\rangle$ because the local polarization is mostly σ_+, but as the atom enters a region where the local polarization is mostly σ_-, the probability of optical pumping increases. Optical pumping is most likely to occur at the antinode of the σ_- standing wave, transferring the atom from the top of a hill of the potential $U_{1/2}$, to the bottom of a well in the potential $U_{-1/2}$. The atom then expends more kinetic energy by climbing out of this potential well, only to be optically pumped to the bottom of another $U_{1/2}$ potential well, etc. On average the atom climbs more hills than it descends and its kinetic energy decreases with time. This powerful physical image is known as "Sisyphus cooling" (Dalibard and Cohen-Tannoudji, 1989).

Based on a semiclassical model, Dalibard and Cohen-Tannoudji (1989) estimated spatially averaged friction and diffusion coefficients, and they predicted atomic temperatures corresponding to a mean kinetic energy of order the modulation depth of the lattice potential. Although this simple treatment explicitly ignores atomic localization on the scale of a wavelength, the result suggests that a substantial fraction of the atoms may be trapped in individual optical potential wells. In that case one can approximate the atomic motion near the bottom of the wells by a simple harmonic oscillator that is thermally excited. Expansion of the optical potential around the minimum of a potential well yields the oscillation frequency ,

$$\hbar\omega_{osc} = 2\sqrt{\frac{2}{3}U_0\,E_R}\ ; \qquad E_R = \frac{\hbar^2 k^2}{2M}, \tag{3}$$

where E_R is the single photon recoil energy and M the atomic mass. Note that it is meaningful to talk about oscillatory atomic motion only if an atom resides in a given potential well for a time at least comparable to the oscillation frequency. This is precisely the regime in which one must describe the atomic center-of-mass motion quantum mechanically as we will see in sect. IV, and also the regime that has been found

experimentally to lead to the lowest temperatures (Lett et al., 1988; Weiss et al., 1989; Salomon et al., 1990).

B. SPECTROSCOPY IN 1D LIN⊥LIN OPTICAL LATTICES

Early experimental work on six-beam optical molasses measured the distribution of atomic momenta (Lett et al., 1988), which contains no direct evidence of atomic localization or oscillatory motion. In the period 1989-1992 several spectroscopic methods were pursued as alternative means of probing the laser cooling process. In the following we briefly introduce the two most successful techniques, deferring a more detailed discussion to sect. V.

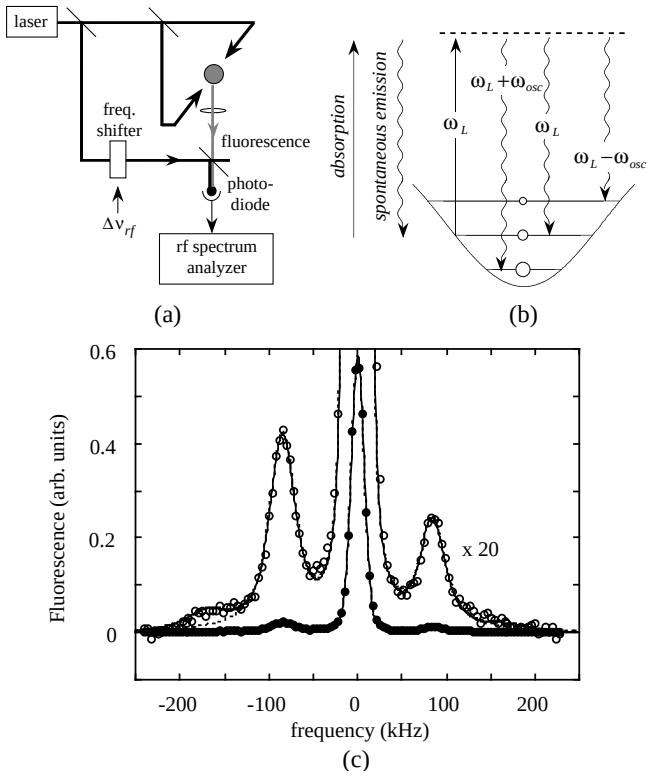

Fig. 2. Fluorescence spectroscopy. (a) Schematic experimental setup. (b) Spontaneous Raman transitions between vibrational eigenmodes of the atomic motion give rise to a Rayleigh line at the optical lattice frequency ω_L and Raman sidebands at $\omega_L \pm \omega_{osc}$. (c) Spectrum of fluorescence measured for ^{85}Rb atoms in a 1D lin⊥lin optical lattice (from Jessen et al. (1992)).

Fig. 2a shows schematically the technique of optical heterodyne spectroscopy of resonance fluorescence developed by the group of Phillips (Westbrook. et al., 1990). Fluorescence emitted by a sample of laser cooled atoms is collected, mixed with a local

oscillator beam and detected by a photo diode. The resulting beat signal is analyzed with a radio-frequency spectrum analyzer, thereby producing a measurement of the power spectrum of the atomic fluorescence. An alternative approach was pioneered by the groups of Salomon, Grynberg, and Kimble, (Grison et al., 1991; Tabosa et al., 1991). This probe spectroscopy technique, Fig. 3a, measures the attenuation of a weak probe beam passing through the atomic sample as its frequency is scanned around the lattice light frequency. Figs. 2c, 3c show fluorescence (Jessen et al., 1992) and probe absorption spectra (Verkerk et al., 1992), respectively, measured for samples of alkali atoms cooled and trapped in a 1D lin⊥lin optical lattice. In both experiments an effective 1D geometry was accomplished by keeping the measurement direction at a very small angle with respect to the lattice axis. Because of considerable laser heating in the plane transverse to the lattice axis, a 1D lattice can be achieved only transiently. Thus the experiments of Verkerk et al. (1992) and Jessen et al. (1992) alternated between measurement periods of a few milliseconds duration with only the 1D lattice present, and periods where an additional superposed 3D molasses was used to cool the transverse atomic motion. As will be discussed, this transient measurement scheme restricts the information available in 1D spectra.

Each set of features in both the fluorescence and probe absorption spectra can be interpreted in related physical terms. We first discuss the fluorescence spectrum shown in Fig. 2c under the assumption that the atomic center-of-mass motion can be described classically. For low saturation, light scattering is predominantly elastic with respect to the atomic internal degrees of freedom, so that the power spectrum of the scattered electric field becomes a delta-function at the laser frequency ω_L, subject to broadening by the atomic motion. An observer seeing the light radiated by the atom would detect a scattered field of the form $\mathbf{E}_s(t) = \frac{1}{2}\mathbf{E}_s e^{-i\omega_L t} e^{-i\Delta k z(t)} + c.c$, where $z(t)$ is the oscillating atomic position and Δk the change in photon wave vector upon scattering. If the atom is harmonically bound, the power spectrum of the radiated light is that of a phase modulated carrier at ω_L with modulation index $\Delta k z_a$, where z_a is the classical oscillation amplitude. Neglecting damping of the atomic motion, the corresponding spectrum is

$$S(\omega) = \sum_{n=-\infty}^{\infty} J_n(\Delta k z_a)^2 \delta[\omega_L + n\omega_{osc}], \tag{4}$$

where $J_n(x)$ is the Bessel function of order n. If the modulation index $\Delta k z_a << 1$, it follows from the properties of the Bessel functions that the amplitude in the nth sideband is of order $(\Delta k z_a)^n$. Therefore the spectrum of Fig. 2c, which exhibits only one pair of strongly suppressed sidebands, is strong evidence that the radiating atoms are well localized in optical potential wells of the 1D lin⊥lin optical lattice. Such tight localization is

comparable with that achieved in ion trapping (Diedrich et al. 1989), and is commonly known as the Lamb-Dicke limit. Because individual lines in the spectrum are well resolved, one can further conclude that the phase diffusion rate of the oscillatory atomic motion is comparable with or less than the oscillation frequency. In other words an atom undergoes, on the average, at least one full oscillation before the phase of oscillation is randomized by photon scattering, or interrupted by optical pumping of the atom to a different internal state. The spectrum shown in Fig. 2c also shows an asymmetry in the power of the red and blue sidebands which cannot be accounted for in the purely classical model, Eq. (4).

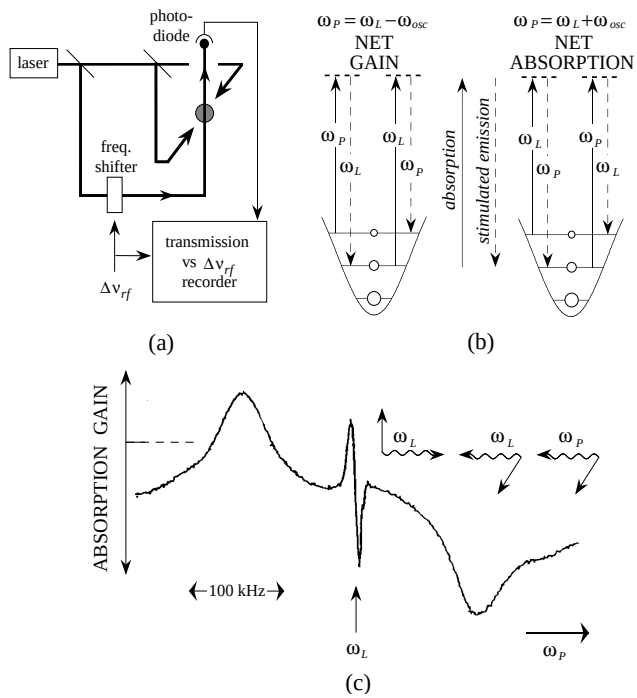

Fig. 3. Probe transmission spectroscopy. (a) Schematic experimental setup. (b) Stimulated Raman transitions between vibrational eigenmodes of the atomic motion redistribute photons between the probe laser at frequency ω_p and the optical lattice at frequency ω_L. Competition between these processes results in net gain for $\omega_P < \omega_L$ and net absorption for $\omega_P > \omega_L$. (c) Probe transmission spectrum measured for ^{133}Cs atoms in a 1D lin⊥lin optical lattice (from Verkerk et al. (1992), reprinted by permission)..

In a quantum theory, the sidebands in the fluorescence and probe absorption spectra of Figs. 2c, 3c can be interpreted in terms of transitions between quantized vibrational states of the atom's center-of-mass motion in a harmonic potential. The fluorescence spectrum contains sidebands at frequencies $\omega_L + \omega_{osc}$ and $\omega_L - \omega_{osc}$ that arise from *spontaneous* Stokes and anti-Stokes Raman transitions of the type illustrated in Fig. 2b, which change

the atom vibrational quantum number by $\Delta n = \pm 1$. For this reason, we refer to these spectroscopic features as "Raman sidebands". In the probe absorption spectrum sidebands arise due to *stimulated* Stokes and anti-Stokes Raman transitions of the type illustrated in Fig. 3b. In such transitions a photon can be either absorbed from or scattered into the probe beam if the Raman resonance condition $\omega_p = \omega_L \pm \omega_{osc}$ is fulfilled. The competition between these two processes determines whether the probe beam experiences net gain or absorption.

Transition rates between vibrational states are readily calculated using Fermi's Golden rule (Wineland and Itano, 1979), yielding $\gamma_{n \to n+\Delta n} \propto \gamma_s \left(k_L z_0\right)^{2|\Delta n|}$ for $\left(k_L z_0\right)^2 = E_R / \hbar\omega_{osc} << 1$, where $\gamma_s \approx \Gamma s_0 / 2$ is the total photon scattering rate and z_0 is the RMS spread of the harmonic oscillator ground state. As in the classical picture we conclude that emission into the sidebands is suppressed if the atoms are well localized on the scale of an optical wavelength (the Lamb-Dicke effect). The observation of well resolved Raman sidebands is due largely to the strong localization, which suppresses the rate of decay of the vibrational populations and coherences.

The asymmetry between red and blue sidebands evident in the fluorescence spectrum is readily accounted for in the quantum model in terms of population differences between vibrational levels. Consider a pair of vibrational states $|n\rangle$ and $|n+1\rangle$ in an optical potential well. In steady state the distribution of population over states is close to thermal, and for any n we have $\Pi_{n+1}/\Pi_n = f_B$, where Π_n is the population of state $|n\rangle$ and $f_B = \exp\left(-\hbar\omega_{osc}/k_B T\right)$ is the Boltzmann factor. Since the rates $\gamma_{n \to n+\Delta n}$ and $\gamma_{n+\Delta n \to n}$ are identical, it follows that Stokes Raman transitions are more frequent than anti-Stokes Raman transitions by a factor f_B. Therefore the oscillator temperature T can be extracted from ω_{osc} and the measured sideband asymmetry. These parameters allow us to determine the mean vibrational excitation $\bar{n}$ and localization Δz of the oscillator. Typical numbers extracted from data such as that of Fig. 2c are $\bar{n} \approx 1$ and $\Delta z \approx \lambda/15$, consistent with atom trapping in the Lamb-Dicke regime.

The central feature at the laser frequency in the fluorescence spectrum arises due to Rayleigh scattering, i. e. Raman transitions that begin and end in the same or a nearly degenerate quantum state. We will defer further discussion of this feature until sect. V. Here we are simply pointing out that in a 1D lattice experiment the width of the Rayleigh line is dominated by Doppler broadening, which occurs because of a small component of the transverse atomic velocity along the measurement direction.

III. Crystallography Of Optical Lattices

An optical lattice of any dimension can be characterized by its crystal structure in a manner analogous to a solid. An extensive discussion of the crystallography of optical lattices for various geometries is given in (Petsas et al., 1994); here we summarize some of the salient features of a few representative lattices. In general, a lattice is defined by a discrete set of vectors, $\{\mathbf{R}_i\}$ such that the potential is invariant under translations, $U(\mathbf{x}+\mathbf{R}_i)=U(\mathbf{x})$. The potential can then be written as a Fourier sum,

$$U(\mathbf{x})=\sum_{\mathbf{K}_j}\tilde{U}_{\mathbf{K}_j}\,e^{i\mathbf{K}_j\cdot\mathbf{x}}. \tag{5}$$

The set of vectors $\{\mathbf{K}_j\}$ define the reciprocal lattice according to the condition $\mathbf{R}_i\cdot\mathbf{K}_j=m2\pi\delta_{ij}$. Although the optical lattice is normally used to trap a single atomic species, the resulting periodic potential is somewhat analogous to the NaCl crystal structure. This subtlety arises from the vector nature of the atom-photon interaction; different atomic "species" correspond to the different internal states of the atom when it is optically pumped by σ_+ or σ_- light. Thus, in general an optical lattice must be described by a Bravais lattice with a basis (Ashcroft and Mermin, 1976). The reciprocal lattice determines the full periodicity of the light field (both intensity *and* polarization); the basis determines the sites of σ_+ and σ_- within the primitive cell.

In the low saturation limit, the light shift is equal to the potential energy stored in a linearly polarizable particle, $U(\mathbf{x})=-\mathbf{E}_L^{(-)}(\mathbf{x})\cdot\vec{\alpha}\cdot\mathbf{E}_L^{(+)}(\mathbf{x})/2$, where $\vec{\alpha}$ is the real part of the atomic polarizability tensor operator and $\mathbf{E}_L^{(+)}(\mathbf{x})$ is the spatial dependence of the laser field's positive frequency component. Given a lattice created by a set of plane waves with equal frequencies, but with arbitrary polarization, direction of propagation, amplitude and phase, we have

$$\mathbf{E}_L(\mathbf{x})=\frac{1}{2}\sum_j E_j\,\vec{\varepsilon}_j\,e^{i(\mathbf{k}_j\cdot\mathbf{x}-\omega_L t+\phi_j)}+c.c.\quad . \tag{6}$$

The optical potential then takes the form,

$$U(\mathbf{x})=-\frac{1}{4}\sum_{j,j'}E_{j'}^{*}E_j\left(\vec{\varepsilon}_{j'}^{\,*}\cdot\vec{\alpha}\cdot\vec{\varepsilon}_j\right)e^{i(\phi_j-\phi_{j'})}\,e^{i(\mathbf{k}_j-\mathbf{k}_{j'})\cdot\mathbf{x}}+c.c.\quad . \tag{7}$$

The potential in Eq. (2) is a special case of (7). In general, the potential is completely specified by the electric field and the atomic polarizability. It is evident by comparison of

Eqs. (5) and (7) that the differences between the wave vectors of the laser beams are reciprocal lattice vectors. It also follows from Eq. (7) that a change in the relative phase between two of the beams, $\phi_j - \phi_{j'}$, is equivalent to an overall translation of the lattice, $\mathbf{x} \to \mathbf{x} + \mathbf{x}_0$. In general the relative phases of the laser beams will fluctuate with time, unless specific steps are taken to prevent this. For b laser beams, there are $b-1$ independent relative phases. Thus, if one wants to create an optical lattice in n dimensions with b laser beams such that the topography of the lattice is constant (apart from n overall translations), one must choose $b=n+1$. This is the approach originally proposed by Grynberg et al. (1993). Typically the fluctuations in the relative phases are slow compared with the atomic response times, so that the trapped atoms adiabatically follow the lattice translations. One can also construct a lattice with time-independent topography by using an arbitrary number of beams with stabilized relative phases; this is the approach used by Hemmerich and Hänsch (1993). In either case, a good optical lattice for trapping atoms will be one where the points of maximum light shift are points of pure σ polarization. In addition, if the lattice is to trap atoms and is tuned near resonance, the net radiation pressure from of the lasers should be zero near the lattice potential minima.

A. Two Dimensional Lattices

Two possible realizations of 2D Grynberg-style lattices are shown in Figs 4(a) and (b). In both cases, the reciprocal lattice is the same, determined only by the differences in the laser wave vectors. The primitive basis for the reciprocal lattice is given by the wave vector differences of maximum magnitude. Assuming θ π/3 gives $\mathbf{b}_1 = \mathbf{k}_2 - \mathbf{k}_1 = K_x\hat{\mathbf{x}} + K_y\hat{\mathbf{y}}$ and $\mathbf{b}_2 = \mathbf{k}_3 - \mathbf{k}_1 = -K_x\hat{\mathbf{x}} + K_y\hat{\mathbf{y}}$, where $K_x \equiv k\sin\theta$, and $K_y \equiv k(\cos\theta + 1)$. In direct space, the primitive cell is spanned by $\mathbf{a}_1 = (\pi / K_x)\hat{\mathbf{x}} + (\pi / K_y)\hat{\mathbf{y}}$ and $\mathbf{a}_2 = -(\pi / K_x)\hat{\mathbf{x}} + (\pi / K_y)\hat{\mathbf{y}}$.

The different polarization choices for these two geometries imply that the basis within a primitive cell, i.e. the relative positions of the σ_+ and σ_- sites, will be different. For configuration A, the positive frequency component of the electric field is given by

$$E_L(\mathbf{x}) = \frac{E_0 e^{-iky}}{\sqrt{2}}\left(-\mathbf{e}_+\left\{1 + 2e^{iK_y y}\cos(K_x x)\right\} + \mathbf{e}_-\left\{1 + 2e^{iK_y y}\cos(K_x x - 2\theta)\right\}\right), \tag{8}$$

where the quantization axis is chosen along $\hat{\mathbf{z}}$, perpendicular to the x-y plane, and the relative phases are chosen such that there is a local maximum of the σ_+ polarized field component at the origin. A basis associated with each primitive cell then consists of a σ_+ site at $\mathbf{v}_1$=0 and a σ_- site at $\mathbf{v}_2 = (2\theta / K_x)\,\hat{\mathbf{x}}$. This 2D configuration will only be a "good

lattice", i. e. have maximum light shift at the points of pure σ polarization, for one choice of angle, θ=π/3. Also, the radiation pressure near the potential minima will vanish for this symmetric geometry. Grynberg et al. (1993) used this lattice to trap Cs atoms in the Lamb-Dicke regime.

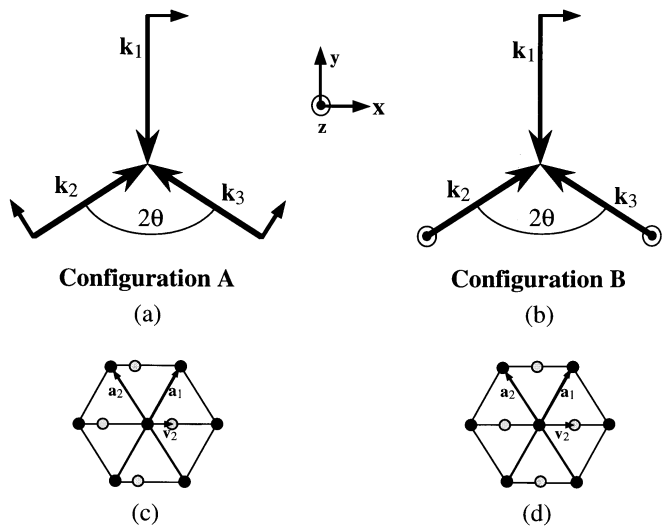

Fig. 4. Two dimensional optical lattice configurations of the Grynberg type, with θ=π/3. (a) and (b) show the configurations of lattice wave vectors and polarization. (c) and (d) show the lattices defined by points of pure σ_+ polarization (black dots) and σ_- polarization (gray dots) for configurations (a) and (b) respectively. The lattices are characterized by a "Bravais lattice with a basis": a primitive cell spanned by a_1 and a_2, and a basis consisting of a σ_+ site at the origin and a σ_- site at v_2.

Consider now configuration B shown in Fig. 4b. We regard this lattice as a 2D generalization of the 1D lin⊥lin geometry, where one of the beams is split into two beams by an angle 2θ. Obtaining the maximum light shift at points of pure σ polarization requires unequal amplitudes of the three plane wave. Choosing $E_2 = E_3 = E_0 / 2$ and a convenient relative phase, the electric field for this geometry is,

$$\mathbf{E}_L(\mathbf{x}) = \frac{E_0 e^{-iky}}{\sqrt{2}}\left(-\mathbf{e}_+\left\{1 + e^{iK_y y}\cos(K_x x)\right\} + \mathbf{e}_-\left\{1 - e^{iK_y y}\cos(K_x x)\right\}\right). \tag{9}$$

Here the quantization axis is chosen in the *x*-*y* plane, along $\mathbf{k}_1$. Unlike configuration A, the radiation pressure at the potential minima is non-zero because of the imbalance in the intensities of the three beams, and so this geometry is not optimal for cooling and trapping in the typical near resonance configuration. However, this geometry always has pure σ

polarization at positions of maximal intensity for an arbitrary angle θ, and therefore retains the possibility of varying the lattice constants through a change in θ, while still maintaining a "good lattice". From Eq. (9) we see that the basis within a primitive cell has σ_+ at $\mathbf{v}_1=0$ and σ_- at $\mathbf{v}_2 = (\pi / K_x)\,\hat{\mathbf{x}}$. Figs. 4(a) and(d) show the lattice structures for configurations A and B with θ=π/3.

Hemmerich and Hänsch (1993) employed a four beam geometry to create a 2D lattice from the interference pattern of an $\hat{\mathbf{x}}$-polarized standing wave along $\hat{\mathbf{y}}$ and a $\hat{\mathbf{y}}$-polarized standing wave along $\hat{\mathbf{x}}$. As we have discussed, this lattice requires phase stabilization to maintain a constant topography. If the relative phase of oscillation of the $\hat{\mathbf{x}}$ and $\hat{\mathbf{y}}$ polarized standing waves is ±π/2 at the antinodes, this represents a "good" lattice with a square primitive cell, reciprocal lattice vectors $\mathbf{b}_1 = k(\hat{\mathbf{x}} + \hat{\mathbf{y}})$ and $\mathbf{b}_2 = k(\hat{\mathbf{x}} - \hat{\mathbf{y}})$, and electric field

$$\mathbf{E}_L(\mathbf{x}) = -\sqrt{2}E_0\left[(\cos kx + \cos ky)\mathbf{e}_+ + (\cos kx - \cos ky)\mathbf{e}_-\right]. \tag{10}$$

B. Three Dimensional Lattices

As in the two dimensional case, there are numerous geometries that one can employ to obtain a "good" three dimensional lattice. Here we discuss a four beam "Grynberg-style" lattice that can be viewed as a three dimensional generalization of the 1D lin⊥lin geometry (Verkerk et al., 1994). Other configurations were discussed by Petsas et al. (1994).

In a manner analogous to the 2D lattice shown in Fig 4b, we imagine starting with a 1D lin⊥lin lattice and "splitting" each of the beams into two, all with equal intensity and in such a way that all polarizations lie in the *x–y* plane, as shown in Fig. 5a. Beams 1 and 2 create an $\hat{\mathbf{x}}$-polarized standing wave along $\hat{\mathbf{y}}$ with a traveling wave component in the $\hat{\mathbf{z}}$-direction, whereas beams 3 and 4 create a $\hat{\mathbf{y}}$-polarized standing wave along $\hat{\mathbf{x}}$ with a traveling wave component in the $-\hat{\mathbf{z}}$-direction. The overall field thus consists of a three dimensional array of σ_+ and σ_- sites (where the quantization axis is chosen along $\hat{\mathbf{z}}$), at positions where the relative phase between the $\hat{\mathbf{x}}$ and $\hat{\mathbf{y}}$ polarized standing waves is ±π/2 (Fig. 5b). Because all beams contribute in equal amplitude to the points of σ polarization, there will be no radiation pressure near the potential minima. There will however be an imbalance in the radiation pressure where the lines of nodes associated with one of the standing waves intersects the lines of antinodes of the other standing wave. This imbalance leads to "escape channels" for untrapped atoms, far from the potential minima.

For simplicity let us consider $\theta_1 = \theta_2 \equiv \theta_L$. The primitive reciprocal lattice vectors are a linearly independent set of laser wave vector differences with the largest magnitude, e.g.,

$\mathbf{b}_1 = \mathbf{k}_1 - \mathbf{k}_3$, $\mathbf{b}_2 = \mathbf{k}_2 - \mathbf{k}_4$, and $\mathbf{b}_3 = \mathbf{k}_3 - \mathbf{k}_2$. In direct space, the spatial dependence of the electric field is

$$\frac{\mathbf{E}_L(\mathbf{x})}{\sqrt{8}E_0} = \left(\hat{\mathbf{e}}_+ \left\{ \cos(k_\parallel z)\left(\frac{\cos(k_\perp y) + \cos(k_\perp x)}{2} \right) + i\sin(k_\parallel z)\left(\frac{\cos(k_\perp y) - \cos(k_\perp x)}{2} \right) \right\} \right.$$
$$\left. + \hat{\mathbf{e}}_- \left\{ \cos(k_\parallel z)\left(\frac{\cos(k_\perp y) - \cos(k_\perp x)}{2} \right) + i\sin(k_\parallel z)\left(\frac{\cos(k_\perp y) + \cos(k_\perp x)}{2} \right) \right\} \right) \tag{11}$$

where $k_\parallel \equiv k_L \cos\theta_L$, and $k_\perp \equiv k_L \sin\theta_L$. Note that in the limit $\theta_L \to \pi/2$, this geometry reduces to the "Hänsch-style" 2D lattice, and Eq. (10) is recovered from Eq (11); as $\theta_L \to 0$ we regain the 1D lin⊥lin geometry. Thus, we see that in the *x*-*y* plane the lattice is square with lattice constant $a_\perp = 2\pi / k_\perp$. Along the *z*–axis, the lattice resembles the 1D lin⊥lin lattice, with a larger lattice constant $a_\parallel = \pi / k_\parallel$. In the nomenclature of crystallography, this lattice is centered tetragonal.

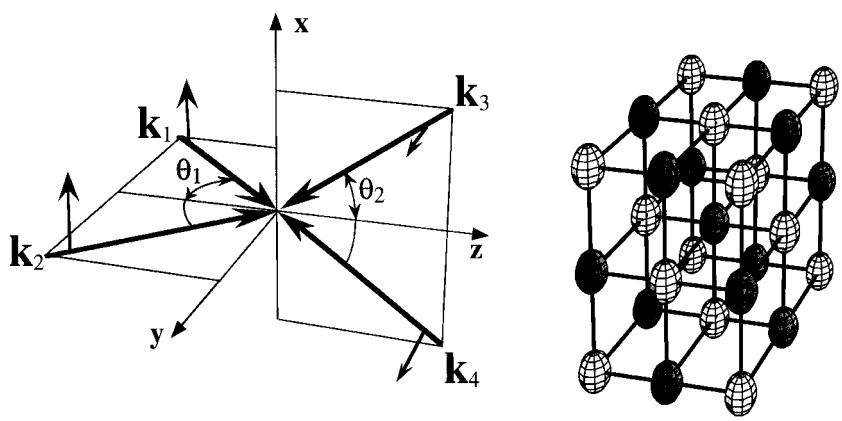

Fig. 5. (a) Grynberg type 3D lin⊥lin lattice. One pair of laser beams travel in the $\hat{\mathbf{y}} - \hat{\mathbf{z}}$ plane ($\mathbf{k}_1$ and $\mathbf{k}_2$), separated by an angle $2\theta_1$, and polarized along $\hat{\mathbf{x}}$. They interfere with another pair that travel in the $\hat{\mathbf{x}} - \hat{\mathbf{z}}$ plane ($\mathbf{k}_3$ and $\mathbf{k}_4$), separated by an angle $2\theta_2$, and polarized along $\hat{\mathbf{y}}$. (b) The resulting centered tetragonal lattice of interleaved σ_+ and σ_- sites.

IV. Laser Cooling In Optical Lattices: Theory

The theory of laser cooling in optical lattices has seen enormous progress over the last few years, involving a synergism of new and old techniques. The close analogy between the periodic potential seen by an electron moving in a solid crystal and the optical lattice potential seen by a laser cooled atom allows us to apply condensed matter formalism to the atomic physics problem. In attempting to solve these models, numerical techniques have

been developed which are not only powerful computational tools, but also give a new understanding of the quantum physics of dissipative systems. In this section we review some of the theoretical models and methods that have been used to study laser cooling in optical lattices and to give interpretations to the experimental results.

A. General Formalism

The general theory of laser cooling of multilevel atoms was discussed in detail by Cohen-Tannoudji (1991) in the Les Houches Summer School. Here we highlight some of the central results. Consider a monochromatic laser field nearly resonant with an atomic transition with ground and excited state angular momenta J_g and J_e. The general description of the system involves the dynamics of $2(J_g + J_e + 1)$ states that evolve coherently through the coupling to the laser field, and dissipatively through the coupling to the vacuum. In the limit of low intensity or large detuning one can reduce the problem significantly; fortunately these are the parameters that lead to the lowest temperatures. In this regime the atomic saturation is small and there is little excited state population. Mathematically, there will then be a separation of time scales - the spontaneous emission time and the optical pumping time - the latter being much longer than the former in the low saturation regime. The excited state populations and atomic coherences between excited and ground states then relax rapidly, and they adiabatically follow the evolution of the ground state manifold. It follows that the excited state variables can be "adiabatically eliminated", leading to a reduced Hamiltonian that acts only on the atom's external coordinates and internal ground state manifold (Castin and Dalibard, 1991),

$$H = \frac{\mathbf{P}^2}{2M} + U_0 \left(\vec{\varepsilon}_L(\mathbf{x}) \cdot \hat{\mathbf{d}}\right)^\dagger \left(\vec{\varepsilon}_L(\mathbf{x}) \cdot \hat{\mathbf{d}}\right), \tag{12a}$$

$$\text{where,} \quad \hat{\mathbf{d}} \equiv \sum_{q, m_g} c_{m_g}^{m_g + q} \left| e; J_e, m_g + q \right\rangle \left\langle g; J_g, m_g \right| \mathbf{e}_q^* . \tag{12b}$$

Here $\mathbf{P}$ and $\mathbf{x}$ refer to the atom's center of mass, $\vec{\varepsilon}_L(\mathbf{x})$ is the laser polarization at $\mathbf{x}$, $c_{m_g}^{m_e}$ is short-hand for the Clebsch-Gordan coefficient coupling the states $\left| J_g, m_g \right\rangle$ and $\left| J_e, m_e \right\rangle$, and $\mathbf{e}_q$ are the spherical basis vectors (q=0,±1).

For geometries where all lattice beam polarization vectors lie in a plane, the field can be decomposed into solely $\sigma_\pm$ components (quantization axis perpendicular to the plane). Consider first an atom with a $J_g = 1/2 \rightarrow J_e = 3/2$ transition as discussed in sect. 2. This system is particularly simple because the $m_g = \pm 1/2$ ground states are not connected by the laser field; this allows us to consider the coherent atomic motion as taking place on one of

two separate *scalar* potentials. This physical picture is too simple if $J_g \geq 1$. Consider therefore an atom with a $J_g = 2 \rightarrow J_e = 3$ transition as shown in Fig. 6a. The light shift operator now contains both diagonal and off-diagonal terms in the basis $|g; J_g, m_g\rangle$; these correspond to absorption and stimulated emission processes with $\Delta m_g = 0$ and $\Delta m_g = \pm 2$ respectively. The $\Delta m_g = \pm 2$ stimulated Raman transitions couple states in families that have m_g either even or odd, as indicated as solid or dotted lines in Fig 6a. If we neglect off-diagonal elements we obtain "diabatic" potentials, whereas if we diagonalize the light-shift operator we obtain "adiabatic" potentials representing the light shift eigenvalues of a stationary atom localized at a particular position. Fig. 6(b) and (c) show the diabatic and adiabatic potentials for a $J_g = 2 \rightarrow J_e = 3$ atom in a 1D lin⊥lin lattice. In general one cannot view the atom as feeling the influence of any single adiabatic or diabatic potential; both are approximations. Slow atoms will follow a single adiabatic potential if the time

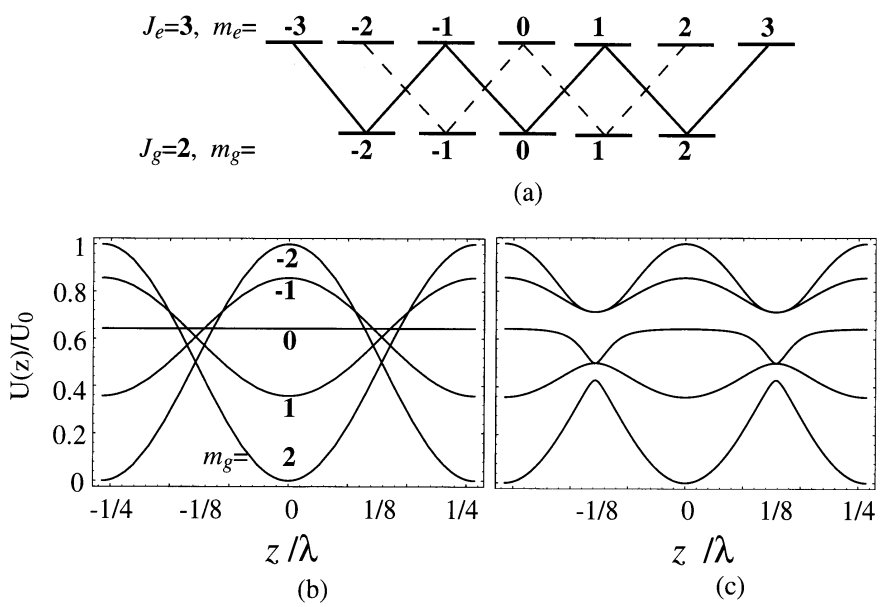

Fig. 6. (a) Level structure of a $J_g = 2 \rightarrow J_e = 3$ atom. The σ_+ and σ_- polarized components of the lattice light field couple the ground state sublevels in families with m_g even (solid lines) and m_g odd (dotted lines). (b) Light-shift eigenvalues as a function position in the 1D lin⊥lin field of Fig. 1a, ignoring coupling between different m_g-states. This yields the diabatic potentials. Numbers next to curves indicate the m_g value. (c) When $\Delta m_g = \pm 2$ coupling between m_g states is included one obtains the adiabatic potentials. The solid curves represent eigenvalues for the coupled "even family" of m_g-states ($m_g = 2, 0, -2$), and the dotted curves for the "odd family" ($m_g = 1, -1$).

spent in the crossing region of the diabatic potentials allows stimulated Raman transitions to occur; fast moving atoms will follow the diabatic potentials. Near the bottom of the optical potential where the polarization is purely $\sigma_\pm$, there is little difference between the adiabatic and diabatic potentials

The above Hamiltonian, Eq (12a) governs only the coherent evolution of the atom. To treat laser cooling one must include dissipative processes, i.e. optical pumping between ground state sublevels. The starting point for most treatments of this problem is the master equation for the atomic density operator ρ following adiabatic elimination of the excited state (Castin and Dalibard, 1991),

$$\frac{d\rho}{dt} = \frac{1}{i\hbar}[H,\rho] - \frac{1}{2}\gamma_s\{\Lambda,\rho\} + \gamma_s \sum_h \int d^2\mathbf{k}_s\, N_h(\mathbf{k}_s)\left(W_h(\mathbf{k}_s)\rho W_h^\dagger(\mathbf{k}_s)\right). \tag{13}$$

The first term is the coherent Schrödinger evolution governed by the Hamiltonian and the last two are the dissipative processes. The second term represent population decay, i. e. depletion of each ground state due to optical pumping into all others, with {,} the anticommutator and the operator $\Lambda \equiv \left(\vec{\varepsilon}_L(\mathbf{x})\cdot\hat{\mathbf{d}}\right)^\dagger\left(\vec{\varepsilon}_L(\mathbf{x})\cdot\hat{\mathbf{d}}\right)$. The third term is a population feeding term due to optical pumping replenishing the populations of each of the ground states. Here the operator $W_h(\mathbf{k}_s) = \left(e^{i\mathbf{k}_s\cdot\mathbf{x}}\,\mathbf{e}_h\cdot\hat{\mathbf{d}}\right)^\dagger\left(\vec{\varepsilon}_L(\mathbf{x})\cdot\hat{\mathbf{d}}\right)$ represents absorption of a lattice photon, followed by emission of a fluorescence photon with wave vector $\mathbf{k}_s$ and helicity h along the quantization axis. The function $N_h(\mathbf{k}_s)$ is the probability distribution for a fluorescence photon with helicity h to propagate along the direction $\mathbf{k}_s$. If one scales all energies by the recoil energy, we see that the master equation depends solely on two dimensionless parameters, $\overline{U}_0 \equiv U_0 / E_R$, and $\bar{\gamma}_s \equiv \hbar\gamma_s / E_R$. The first parameter determines the time scale for the coherent processes such as the oscillation of atoms deeply bound at the bottom of the wells, and the second determines the time scale for the dissipative processes such as optical pumping. In principle, all information is contained within Eq. (13), which is an exact description of the atom-laser dynamics in the low saturation limit. Solutions to this equation are not, however, obtained trivially. In the remainder of this chapter we outline some of the various approaches, their advantages and limitations, and the physical insight they give.

B. SEMICLASSICAL METHODS

The master equation (13) is a complete quantum description of the atomic dynamics, including external degrees of freedom. In certain circumstances, one can simplify the problem by treating the center of mass coordinates as classical variables. This *semi-*

classical approximation is valid when the spread in Doppler shifts due to the quantum uncertainty in momentum is small compared with the natural linewidth, and when the spatial coherence length of the atomic wave function is small compared with the optical wavelength. In addition the internal degrees of freedom must relax much faster than the external degrees of freedom so that one can treat the atom as a classical particle experiencing an instantaneous force. For multilevel atoms in optical lattices the semiclassical approximation typically breaks down, not because the atomic wave function has spatial coherence over distances larger than the optical wavelength, but because the internal time scale τ_{int} becomes much longer than the external time scale τ_{ext}. Consider an atom tightly bound in a σ_+ potential well. The atomic localization reduces the overlap of the atomic center-of-mass distribution with the σ_- polarized standing wave by a factor of order the Lamb-Dicke parameter $\left(E_R/\hbar\omega_{osc}\right)$. This reduces the rate of optical pumping, so that $\tau_{int} \approx \left[\left(E_R/\hbar\omega_{osc}\right)\gamma_s\right]^{-1} >> \omega_{osc}^{-1} \approx \tau_{ext}$, where the inequality is fulfilled as soon as $\Delta/\Gamma >> 1$. This parameter regime is known as the "oscillating regime", whereas the reverse situation, $\tau_{int} << \tau_{ext}$, is known as the "jumping regime". Various procedures have been employed to recover an approximate semiclassical equation of motion in the oscillating regime (Castin et al., 1991; Castin et al., 1994). Some system properties can be deduced using such models, but they fail to account for purely quantum effects such as tunneling. For this reason a full quantum theory, including the external degrees of freedom, is necessary.

C. THE MONTE-CARLO WAVE FUNCTION TECHNIQUE

A brute force solution of the master equation would involve expanding the density operator in an appropriate basis including $2J_g + 1$ internal states and a large number of external states. In principle, the external degrees of freedom have a continuous spectrum, but they can be restricted to a grid consistent with the desired resolution in momentum space. Even for a typical 1D laser cooling problem, the dimension of the Hilbert space, *N*, can be on the order of $10^3 - 10^4$. The corresponding density matrix has $N^2 = 10^6 - 10^8$ elements, and numerical solution of Eq. (13) becomes intractable even for sparse matrices. Given these difficulties, the groups of Mølmer, et al. (1993) and of Zoller (Marte et al., 1993a) have applied a Monte-Carlo wave function simulation technique to the problem. The essence of this method is to view the density operator as an ensemble average of "quantum trajectories". Because wave functions have only *N* elements, compared to the density matrix which has N^2 elements, the technique leads to considerable savings in computer memory. The tradeoff is that extra computer time is needed to simulate a large number of trajectories. Each trajectory consists of the deterministic evolution of a wave

function punctuated by quantum jumps at random times. The stochastic evolution represented by quantum jumps originates from the coupling of the small quantum system at hand to a large reservoir. For our case, the small system consists of an atom, and the role of the reservoir is played by vacuum fluctuations. Not only is the Monte-Carlo method a useful computational tool, it gives physical insight into the quantum mechanics of dissipative systems. Many other problems in quantum optics have been studied by similar formulations in which the master equation is replaced by stochastic equations (Gardiner et al., 1992; Gisin and Percival, 1992; Carmichael, 1993).

In a beautiful application of this technique, Marte et al. (1993b) calculated the fluorescence spectrum of Rb atoms laser cooled in a 1D lin⊥lin lattice, and found spectacularly close quantitative agreement with experiments. The calculated spectrum shows well resolved Raman sidebands that are suppressed by the Lamb-Dicke effect, as discussed in sect. II, and reproduces the sideband asymmetry that reflects the distribution of population over vibrational states. Castin et al. (1994) have used the Monte-Carlo simulations to calculate the steady state properties of $J_g = 1/2 \rightarrow J_e = 3/2$ atoms in a 2D lattice, in general agreement with other methods described in what follows. Castin and Mølmer (1995) have also applied this technique to a 3D optical molasses in the standard six beam configuration. Their system was effectively an optical lattice, since a particular phase relation between the beams was chosen for the simulation.

In translating the master equation into a set of stochastic equations of motion, the basis of decomposition should be chosen appropriately for the application at hand. For studying velocity distributions, the natural basis are energy eigenstates, which are delocalized. On the other hand, if one studies spatial diffusion of atoms in a lattice, the natural basis would consist of localized states. Such an approach was initiated by Holland et al. (1996), using wave functions that represent the diffraction limited images of an atom viewed through the photons it emits into a lens with a large aperture (the Heisenberg microscope). They applied this technique to calculate the diffusion of atoms in a one dimensional optical lattice. The spatial trajectory of the atom shows long periods in which the atom is trapped near a given lattice site, punctuated by long "flights" over many wavelengths when energy fluctuations allow the atom to "boil" out of a well. The spatial diffusion coefficient was calculated for atoms driven on a $J_g = 1/2 \rightarrow J_e = 3/2$ transition, and found to be an order of magnitude larger than for atoms driven on a $J_g = 3 \rightarrow J_e = 4$ transition. This indicates that atoms with large angular momentum are trapped for longer times in the wells; more research is however necessary to extend the standard model of Sisyphus cooling and to understand the mechanism by which this trapping occurs. The nature of the trajectories has an interesting statistical features which has analyzed in terms of Lévy-flights by Marksteiner et al. (1996).

D. BAND STRUCTURE FORMALISM

A full quantum theory of laser cooling in optical lattices starts with the Hamiltonian in Eq. (12a), where now the external coordinates (**x**,**P**) are quantum operators. Because the Hamiltonian is invariant under translations by any lattice vector **R**, as described in sect. 3, the energy eigenstates must satisfy Bloch's theorem. This is analogous to the description of an electron moving in the periodic potential formed by the ionic cores in a solid. The resulting energy spectrum consist of bands, with a large bandgap separating the tightly bound states, and a quasicontinuous spectrum for free states. In the oscillating regime, laser cooling can be analyzed by first diagonalizing the laser-atom Hamiltonian, and then treating the vacuum as a perturbation. This procedure is somewhat analogous to the dressed state treatment of resonance fluorescence of atoms in intense laser fields (Cohen-Tannoudji et al., 1992). The master equation (13) then governs the populations in Bloch states and coherences between them. In a near-resonant lattice, spontaneous emission will destroy the spatial coherence of the atomic wave function over distances large compared to the optical wave length and therefore the steady state density matrix will be a statistical mixture of Bloch states with a limited coherence length.

We begin with the diagonalization of the atom-laser Hamiltonian, Eq. (12a). The physical problem differs somewhat from the standard solid state problem, in part because the optical potential depends strongly on the internal state of the particle, and in part because the internal and external degrees of freedom are not generally separable. As a consequence the eigenstates are "entangled states" of these variables, rather than product states. In general one can write the state of the atom as a $2J_g+1$ component spinor. Each wave function is then expressed in Bloch form as

$$|\psi\rangle = \sum_{m_g} e^{i\mathbf{q}\cdot\mathbf{x}} \left|u_{\mathbf{q}}^{m_g}\right\rangle \otimes \left|m_g\right\rangle, \tag{14}$$

where $\left|u_{\mathbf{q}}^{m_g}\right\rangle$ has the periodicity of the lattice. A special, simple case is that of a 1D lin⊥lin lattice driving a $J_g = 1/2 \rightarrow J_e = 3/2$ transition. The energy eigenstates are diagonal in the basis of m_g–states as previously described and the problem reduces to two independent scalar problems. The band structure for this system was calculated by Castin and Dalibard (1991).

Consider now a 1D lin⊥lin lattice driving a $J_g = 2 \rightarrow J_e = 3$ transition as shown in Fig. 6a. A brute force approach would be to substitute the spinor representation, Eq. (14), into the Hamiltonian, and diagonalize it to obtain eigenenergies and eigenstates. This task is simplified by careful consideration of the symmetries of the Hamiltonian (Castin, 1992;

Courtois, 1993). The basic symmetry $T_{\lambda/2}$, consisting of a translation by λ/2, is built into the Bloch states. In addition, one immediately finds that the Hamiltonian is block diagonal, with even m_g in one block, and odd m_g in the other. This separation arises from a rotation symmetry of the system about the *z*-axis by 180°. The unitary operator associated with this symmetry is $R = \exp\{-i\pi J_z\}$, with eigenvalues $\eta = (-1)^{m_g} = \pm 1$ corresponding to the two "families" of m_g-states. We can now solve the problem for each family η separately. Diagonalizing the Hamiltonian for a given η, one finds that for each quasimomentum q the eigenvalues come in pairs, which are nearly degenerate for tightly bound states and have increased energy separation for higher lying states. For integer angular momentum, these pairs are associated with a third symmetry of the problem, $\tau \equiv T_{\lambda/4} \otimes \sum_{m_g} |-m_g\rangle\langle m_g|$, corresponding to translation by λ/4 and a mapping $m_g \to -m_g$. Since $\tau^2 = T_{\lambda/2}$, one sees that τ has eigenvalues $\zeta e^{iq\lambda/4}$, where $\zeta = \pm 1$.

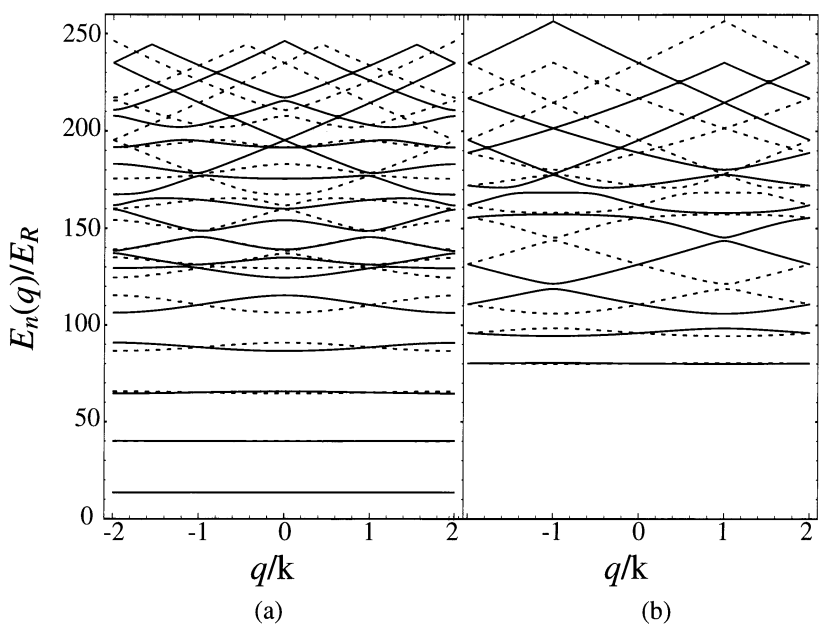

Fig. 7. Band structure in the first two Brillouin zones for a $J_g = 2 \to J_e = 3$ atom driven by a 1D lin⊥lin optical lattice, with a maximum light shift $U_0 = 200E_R$. (a) The energy eigenvalues associated with the family of even m_g-states ($\eta = 1$).(b) The energy eigenvalues associated with the family of odd m_g-states ($\eta = -1$). Solid and dotted lines represent bands with parity eigenvalue ζ =+1 or –1 respectively.

Each pair of eigenfunctions represent even and odd parity solutions of the wave function between neighboring wells of opposite helicity. The energy eigenstates $|n, q, \eta, \zeta\rangle$ are thus simultaneous eigenfunctions of the four mutually commuting operators $\{H, T_{\lambda/2}, R, \tau\}$.

There is yet a fourth symmetry of the Hamilton: parity together with a rotation by 90° about the z-axis, $I = P \otimes e^{-i\pi J_z/2}$. I does not commute with the translation operator, however one can show $I|n,q,\eta,\zeta\rangle = \pm\sqrt{\eta}|n,-q,\eta,\eta\zeta\rangle$, from which it follows that the energy bands satisfy $E_{n,q,\eta,\zeta} = E_{n,-q,\eta,\eta\zeta}$.The diagonalization procedure involves choosing a value for q, η, and ζ, and substituting the representation Eq. (14) into the Hamiltonian. The band structure for $U_0 = 200E_R$ is shown in Fig. 7. As compared with the $J_g = 1/2 \rightarrow J_e = 3/2$ transition, the energy bands exhibit substantial curvature for states closer to the bottom of the potential wells. This curvature arises because atoms with angular momentum $J_g \geq 1$ can tunnel between neighboring wells of opposite polarization. The band curvature becomes substantial as soon as the energy rises above the top of the lowest adiabatic potential well (Fig. 6c). Such bands do not, however, have completely free particle character, indicating the mixed adiabatic/diabatic nature of the potential.

E. THE SECULAR APPROXIMATION

Given the energy band structure described above, one can expand the master equation, Eq. (13) in the basis of the Bloch states. If we are interested only in the steady state solution, some simplifications can be made. We first note that all of the symmetries of the Hamiltonian, $T_{\lambda/2}, R, \tau, I$, are also symmetries of the dissipative part of the master equation, implying that the steady state density operator must be invariant under these unitary operations. Therefore no off-diagonal matrix elements between states of different q, η, or ζ survive. Consider the steady state master-equation for a matrix element between two states of different energy bands, all other eigenvalues being the same,

$$\dot{\rho}_{nn'} = \frac{1}{i\hbar}\left(E_n - E_{n'}\right)\langle n|\rho|n'\rangle + \gamma_s \langle n|\mathcal{L}_{\text{relax}}[\rho]|n'\rangle = 0, \tag{15}$$

where $\mathcal{L}_{\text{relax}}[\rho]$ is the dissipative part of the master equation. For the tightly bound states, the energy spectrum closely approximates a simple harmonic ladder with energy spacing $E_{n+1} - E_n = \hbar\omega_{osc}$. In the "oscillating regime", $\omega_{osc} >> 1/\tau_{pump}$, the energy spacing is much larger than the incoherent linewidth. Then the first term in Eq. (15) will be much larger than the second, and therefore in steady state we must have $\langle n|\rho|n'\rangle \approx \rho_{nn'}\delta_{nn'}$ for tightly bound states. In this so-called *secular approximation*, the master equation reduces to a set of rate equations for population transfer between the Bloch states (Castin, 1992),

$$\dot{\Pi}_{nq\eta\zeta} = -\gamma_{nq\eta\zeta}\,\Pi_{nq\eta\zeta} + \sum_{n'q'\eta'\zeta'} \gamma_{n'q'\eta'\zeta' \rightarrow nq\eta\zeta}\,\Pi_{n'q'\eta'\zeta'}, \tag{16}$$

where $\gamma_{nq\eta\zeta} = \gamma_s \langle nq\eta\zeta|\Lambda|nq\eta\zeta\rangle$ is the total departure rate from the state $|nq\eta\zeta\rangle$, and

$$\gamma_{n'q'\eta'\zeta'\to nq\eta\zeta} = \gamma_s \int_{-k}^{k} dk_s\, N(k_s) \sum_h \left|\langle nq\eta\zeta|W_h(k_s)|n'q'\eta'\zeta'\rangle\right|^2 \tag{17}$$

is the rate of optical pumping between states. Multiplying γ_s is the Franck-Condon factor, accounting for both conservation of linear and angular momentum in the transition. Conservation of the total population is ensured by the fact that $\gamma_{nq\eta\zeta} = \sum' \gamma_{n'q'\eta'\zeta'\to nq\eta\zeta}$.

The symmetries of the system determine certain selection rules for optical pumping, which in turn limit the number of nonvanishing transition matrix elements that must be calculated. For example, the transition matrix element between two Bloch states in a 1D lattice is nonvanishing only for $q - q' = \pm k_L + \mathbf{k}_s \cdot \hat{\mathbf{z}}$. This is a statement of momentum conservation. Since photons can be spontaneously emitted along any direction, the recoil along the *z*-axis spans all values and therefore couples all quasimomenta *q* within a band. This complete description makes the problem numerically intractable and one typically simplifies the spontaneous emission pattern to match the symmetry of the lattice. Solving for the steady state populations in the various Bloch states is then straightforward. One chooses a finite but sufficient number of bands and calculates the transition rates between them according to Eq. (17). Given the conservation of the total population, one can then invert the rate equation matrix when the left hand side is set to zero.

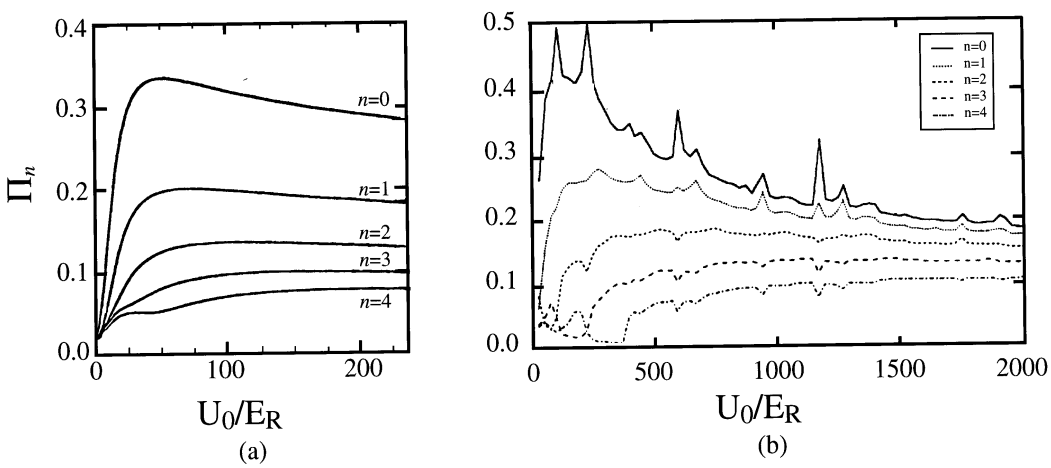

Fig. 8. (a) Steady state populations in the first five energy bands for a $J_g = 1/2 \to J_e = 3/2$ transition (from Castin 1992, reprinted with permission). (b) Steady state populations in the first five energy bands for a $J_g = 4 \to J_e = 5$ transition (from Courtois 1993, reprinted with permission). Both figures are for a 1D lin⊥lin optical lattice, and show populations as a function of the maximum light shift U_0.

Fig 8a shows the steady state population of the first 5 energy bands for a $J_g = 1/2 \rightarrow J_e = 3/2$ transition as a function of total light shift, with a total of 80 bands included in the rate equations, as calculated by Castin and Dalibard (1991). The population of the lowest band reaches a maximum value of 34% of the total population, with only 20% of the population in the quasi-free bands. This suggests that atoms are indeed strongly localized in the optical potential wells. The rate equation approach has also been used to calculate properties of higher angular momentum atoms in a 1D lin⊥lin lattice, with the more complex band structure described previously. Fig. 8b shows the steady state populations for cesium ($J_g = 4 \rightarrow J_e = 5$), as calculated by Courtois (1993). Sharp resonances appear in the populations of the lowest band at specific values of the light shift. These have been interpreted as arising from strong transfer of population to the ground state when energy bands associated with one of the high lying adiabatic potentials matches that of the deepest potential. Such resonances have also been predicted to occur in a 2D optical lattice, when bound states of neighboring wells of different character are resonant (Berg-Sørensen et al., 1993).

The rate equation approach to laser cooling in optical lattices has been applied to numerous other systems. Doery et al. (1994) have used band theory to study the velocity distribution of $J_g = 1/2 \rightarrow J_e = 3/2$ atoms in both a 1D lin⊥lin lattice and in a 1D σ_+ standing wave with a magnetic field. Castin et al. (1994) have calculated the steady-state properties of $J_g = 1/2 \rightarrow J_e = 3/2$ atoms in a 2D "Hänsch-style lattice" described in sect. III, and Berg-Sørensen (1994) has done a similar calculation for a "Grynberg-style" 2D lattice. The minimum temperatures in these lattices is of the same order as the 1D lin⊥lin case, with the added feature that tunneling resonances may appear for certain parameters. To date, no calculations of this type have been performed on large angular momentum atoms in higher dimensional lattices.

V. Spectroscopy

Spectroscopy has been the method of choice for probing the quantized atomic motion and cooling dynamics in optical lattices. Sect. II briefly introduced resonance fluorescence and probe transmission spectroscopy; in addition phase conjugation spectroscopy (Lounis et al., 1993; Hemmerich et al., 1994a), which measures the frequency dependent phase conjugate reflection of a probe beam, has been employed in the study of optical lattices. These techniques probe atoms in an optical lattice through the interaction between the atomic dipole moment $\mathbf{d}$ and the electromagnetic field. In fluorescence spectroscopy one measures the spectrum of fluctuations of $\mathbf{d}$, driven by the coupling of the atomic dipole to the lattice field and vacuum modes. In probe absorption or phase conjugation spectroscopy

an external probe field drives the system, resulting in energy exchange between the probe and lattice fields.

In sect. IV we showed that the evolution of the atomic system is described by the master equation (13). We can write Eq. (13) in matrix from as $\dot{\mathbf{S}} = \mathcal{L}\mathbf{S}$, where $\mathbf{S}$ is the Bloch vector containing the elements of the density matrix, and $\mathcal{L}$ is the super-operator governing the evolution of $\mathbf{S}$. A representation can be chosen in which $\mathcal{L}$ is diagonal, in which case the evolution of $\mathbf{S}$ is trivially determined. It follows that the normal modes associated with the dynamical evolution of the system are eigenvectors of $\mathcal{L}$, and that the kth normal mode evolves as $e^{\lambda_k \tau}$, where λ_k is the corresponding eigenvalue. Optical lattice parameters are often close to the secular regime, so that the normal modes of the system remain close to the basis states of Eq. (14) and the system dynamics can be discussed in terms of transitions between those states. As outlined in sect. II, this often allows a simple physical interpretation of the spectrum in terms of Raman and Rayleigh processes.

A. SPECTROSCOPIC TECHNIQUES

1. Fluorescence Spectroscopy

The normalized power spectrum of the fluorescence electric field is, by definition, the Fourier transform of the normalized first order correlation function $g_s^{(1)}(\tau) = \langle\, \hat{\varepsilon}_D^* \cdot \mathbf{E}_s^{(-)}(t+\tau)\, \hat{\varepsilon}_D \cdot \mathbf{E}_s^{(+)}(t)\,\rangle / I_s$, where $\hat{\varepsilon}_D$ is the detection polarization, and I_s is the scattered intensity. The scattered field, $\mathbf{E}_s^{(\pm)}(t)$, is proportional to $\mathbf{d}^{(\pm)}(t - r/c)$, where r is the atom-detector distance. It follows that $g_s^{(1)}(\tau)$ is also the normalized correlation function of the atomic dipole. The quantum regression theorem states that the evolution of averages of the type $g_s^{(1)}(\tau)$ is governed by the same equation of motion as that of the Bloch vector $\mathbf{S}$ (Cohen-Tannoudji et al., 1992), so that

$$g_s^{(1)}(\tau) = e^{i\omega_L \tau} \sum_k c_k\, e^{\lambda_k \tau} \;;\; \tau \geq 0\,. \tag{18}$$

In this expression $\{\lambda_k\}$ are the eigenvalues of the super-operator $\mathcal{L}$, and $\{c_k\}$ are complex amplitudes that are in principle calculable. Equation (18) shows that in the secular regime the spectrum is the sum of Lorentzian lines with amplitudes $\mathrm{Re}[c_k]$, center frequencies $\omega_L + \mathrm{Im}[\lambda_k]$, and half-widths $\mathrm{Re}[\lambda_k]$ that are small compared with the line separations. In this limit one can associate each line with transitions between a particular set of states, and determine the amplitudes $\mathrm{Re}[c_k]$ from rate equations. Some general information about the nature of the spectrum is available from the properties of $\mathcal{L}$. Because a representation can be chosen in which $\mathcal{L}$ is real, the eigenvalues are either real or come in pairs $\lambda_k = \lambda_{k'}^*$. Consequently the spectrum contains components at $\omega_L \pm \mathrm{Im}[\lambda_k]$ with identical widths, but

since possibly $c_k \neq c_{k'}^*$ the spectrum need not be symmetric around ω_L. If the system is closed, $Tr(\rho)=1$, a representation may be chosen in which one of the elements of $\mathbf{S}$ is constant. The corresponding eigenvalue is zero and the corresponding eigenvector is the normal mode associated with the steady state; this is the source of the coherent component in the spectrum.

The group of Phillips have demonstrated an optical heterodyne technique for spectrum analysis of resonance fluorescence (Westbrook et al., 1990; Jessen et al., 1992). The technique is illustrated in Fig. 2a, and was discussed briefly in sect. II. Light radiated by atoms in the optical lattice is combined with a local oscillator beam, and interferes to produce a total electric field $\mathbf{E}_{tot}(t)=\hat{\varepsilon}_D E_{LO}\cos(\omega_{LO}t)+\mathbf{E}_s(t)$. For the moment we consider these fields to be classical. The total intensity of the interfering fields is measured with a photodiode, resulting in a current

$$i(t) \propto \left|\mathbf{E}_{tot}(t)\right|^2 \propto \left|E_{LO}\right|^2 + \mathrm{Re}\left[\mathbf{E}_s(t)^* \cdot \hat{\varepsilon}_D E_{LO} e^{-i\omega_{LO}t}\right], \tag{19}$$

where terms that are second order in $\left|\mathbf{E}_s(t)\right|$ and terms that oscillate at optical frequencies have been omitted. The physical significance of the remaining terms is as follows: the term $\left|E_{LO}\right|^2$ produces a DC component in the spectrum, as well as shot noise due to the quantization of the photo-current; the term $\mathbf{E}_s(t)^* \cdot \hat{\varepsilon}_D E_{LO} e^{-i\omega_{LO}t}$ is the signal of interest. The power spectrum of the current for $\omega \geq 0$ is

$$\begin{aligned} P_i^{\text{meas.}}(\omega) = & \frac{e i_{LO}}{\pi} + 2 i_{LO}{}^2 \delta(\omega) \\ & + \frac{i_{LO}\langle i_s(t)\rangle}{\pi}\int_{-\infty}^{\infty} \exp(i\omega_{LO}\tau) g_s^{(1)}(\tau)\exp(-i\omega\tau) d\tau \end{aligned}, \tag{20}$$

where i_{LO} and i_s are the separate currents generated by the local oscillator and signal light. Equation (20) shows that the measured power spectrum of the photo-current contains 3 contributions: a frequency independent shot-noise background, a DC current generated by the local oscillator, and a signal term that is an exact replica of the power spectrum of $\hat{\varepsilon}_D \cdot \mathbf{E}_s(t)$, translated to an rf intermediate frequency $\left|\omega_{LO}-\omega_L\right|$.

The primary technical concerns in optical heterodyne spectroscopy are frequency resolution and signal-to-noise ratio (S/N). Westbrook et al. derived both the local oscillator and optical lattice beams from the same laser, in which case the measurement setup of Fig 2a is equivalent to a Mach-Zender interferometer, with atoms in the lattice playing the role of a mirror. It is well known that such an interferometer has good fringe visibility as long as the optical path difference in the interferometer is much smaller than the laser coherence

length. Typical laser sources employed in laser cooling therefore contribute negligibly to the frequency resolution, which in practice is limited by mechanical mirror vibration. Obtaining a useful S/N in a measurement of the spectrum is usually a much more serious concern. Jessen (1993) has performed a detailed analysis of S/N issues in optical heterodyne fluorescence spectroscopy; here we note only that since the rate of photon scattering $\gamma_s \propto 1/\Delta^2$, a useful S/N in fluorescence spectroscopy has been achieved only for moderate detunings $|\Delta| \lesssim 10\Gamma$.

Photon correlation or self-heterodyne spectroscopy measures the power spectrum of the photo-current generated by the fluorescence without a local oscillator beam. In that case the photo-current correlation function is a replica of the second order correlation function $g_s^{(2)}(\tau)$ of the scattered field. If the photon statistics of the source is Gaussian, one can use the relation $g_s^{(2)}(\tau) = 1 + \left|g_s^{(1)}(\tau)\right|^2$ to partly recover $g_s^{(1)}(\tau)$. Because the phase of $g_s^{(1)}(\tau)$ is not available, the power spectrum of the photo current is centered on DC and information about the asymmetry of the spectrum is lost. Considerations of resolution and S/N are essentially the same as for heterodyne detection. Photon correlation spectroscopy has been applied recently to an atomic sample in a magneto-optic trap (Jurczak et al., 1995).

2. Probe Spectroscopy:

By applying a probe to the system at frequency ω_p, one can measure either the transmitted signal or the phase-matched phase conjugate reflection (via four wave mixing) as a function of $\delta_P = \omega_P - \omega_L$. Typically the probe is weak and its only effect is to excite particular normal modes of the unperturbed system (Courtois and Grynberg, 1992). As discussed, the normal modes are the eigenvectors of the super-operator $\mathcal{L}$ that governs the evolution of the atom/lattice system in the absence of the probe. The transfer of energy between the probe field and the atom/lattice system is most efficient when δ_P corresponds to a particular dynamical evolution frequency $\mathrm{Im}[\lambda_k]$. Thus the information contained in the probe transmission and phase conjugation spectra is largely equivalent to the information in the fluorescence spectrum. In the secular regime one can associate features in the spectra with stimulated Raman transitions between system eigenstates that lead to redistribution of photons among lattice and probe beams. As discussed in sect. II, the net amount of gain and absorption at a given frequency is determined by the competition between stimulated Raman processes that involve lattice and probe photons in opposite order, as illustrated in Fig. 3b. Thus the gain/absorption of a probe beam passing through the lattice is proportional to the total population difference between the coupled states. It follows that the pair of Raman lines at frequencies $\omega_L \pm \mathrm{Im}[\lambda_k]$ is antisymmetric; a gain of α at frequency $\omega_L - \mathrm{Im}[\lambda_k]$ is accompanied by an absorption of $1/\alpha$ at frequency $\omega_L + \mathrm{Im}[\lambda_k]$. In general the probe transmission through a medium without population

inversion will exhibit gain for $\omega_p < \omega_L$ and absorption for $\omega_p > \omega_L$, as is the case in Fig. 3c.

The frequency resolution that can be achieved in probe spectroscopy is subject to the same limitations as fluorescence spectroscopy, whereas the problem of achieving useful S/N is less severe. The difference in the S/N ratio of these two techniques can be explained as follows. In probe spectroscopy, emission of a probe photon is *stimulated* by the lattice/probe beams, whereas the fluorescence is *spontaneous* emission. Viewed classically, in probe spectroscopy the atomic motion is coherently driven by the interference of probe and lattice fields, and therefore the light scattered from each atom constructively interferes. In fluorescence spectroscopy, the atomic motion is incoherently driven by the lattice and vacuum fields, and light emitted from different atoms does not interfere constructively. This results in a much weaker scattered field.

B. EXPERIMENTAL RESULTS

The first spectroscopic measurements on laser cooled atoms were performed by Westbrook et al. (1990) who found evidence of localization of Na atoms in the optical potential wells of a 3D molasses. This work was followed by that of Verkerk et al. (1992) and Jessen et al. (1992) who studied 1D lin⊥lin optical lattices as discussed in sect. II. At this time Gupta et al. (1992) were independently studying the 1D lin⊥lin lattice configuration by rf spectroscopy; physical understanding of this type of measurement was however complicated by the high rf fields necessary to drive the electric-dipole forbidden one-photon transitions between bound states of the lattice. Insight gained from these experiments also permitted the extension to 2D and 3D lattice configurations as reported by Grynberg et al. (1993) and Hemmerich and Hänsch (1993). Since then spectroscopy has been performed on a wide range of lattice configurations. Generally one finds closely analogous features in fluorescence and probe spectroscopy, i.e. Raman sidebands and a Rayleigh line. In the following we organize our discussion so as to address the experimental findings for each of these features in turn.

1. Raman sidebands

As discussed in sect. II, resolved Raman sidebands in the fluorescence and probe spectra are characteristic of a well designed optical lattice. These spectroscopic features may be interpreted in terms of spontaneous or stimulated Raman transitions between eigenstates of the atomic center-of-mass motion. In the following we restrict the discussion to the secular regime, where the position of Raman lines in the spectrum correspond to transition frequencies of the system. Strictly speaking the eigenstates of the system are the

Bloch states, Eq. (14). However because long-range coherence is destroyed by spontaneous emission, localized states form a more appropriate basis in which to discuss the spectra. Consider therefore a highly localized state in a σ_+ potential well of the lowest adiabatic potential of Fig. 6c, belonging to a 1D lin⊥lin lattice. Tightly bound atomic states approximately factorize as $\left|J_g, m_g\right\rangle \otimes |n\rangle \otimes \left|\mathbf{p}_\perp\right\rangle$, where m_g is the maximum magnetic quantum number, $|n\rangle$ is a harmonic oscillator state, and we characterize the free atomic motion transverse to the lattice by the state $\left|\mathbf{p}_\perp\right\rangle$. Optical pumping transfers most of the population to these states and light scattering then occurs mainly on the closed $\left|J_g, m_g\right\rangle \leftrightarrow \left|J_e, m_g+1\right\rangle$ transition. This suggests that the spectra may reasonably be interpreted in terms of a harmonically bound 2-level atom. The transition rate, Eq. (17), due to scattering of lattice light into the direction $\mathbf{k}_s$ is approximately

$$\begin{aligned}\gamma_{n,\mathbf{p}_\perp \to n',\mathbf{p}'_\perp} &\approx \gamma_s \left|\left\langle n', \mathbf{p}'_\perp \right| e^{i\mathbf{k}_s\cdot\mathbf{r}} \cos\left(\mathbf{k}_L \cdot \mathbf{r}\right) \left| n, \mathbf{p}_\perp \right\rangle\right|^2 \\ &\approx \gamma_s \left(\delta_{n,n'}\, \delta(\mathbf{p}'_\perp - \mathbf{p}_\perp, \hbar\Delta\mathbf{k}_\perp) + \left|\left\langle n', \mathbf{p}'_\perp \right| \mathbf{k}_s \cdot \mathbf{r} \left| n, \mathbf{p}_\perp \right\rangle\right|^2 \delta_{n,n'\pm 1}\, \delta(\mathbf{p}'_\perp - \mathbf{p}_\perp, \hbar\Delta\mathbf{k}_\perp) + \ldots\right)\end{aligned} \tag{21}$$

where $\hbar\Delta\mathbf{k}_\perp$ is the momentum transfer in the transverse plane. The first term in Eq. (21) corresponds to Doppler broadened Rayleigh scattering, whereas the second represents an inelastic process changing the vibrational quantum number by one. The Taylor expansion of the photon modes is valid when the spatial extent of the atom is small compared with the optical wave length, as is true for tightly bound atoms. Note that in lowest order in the Lamb-Dicke parameter $E_R / \hbar\omega_{osc}$, inelastic scattering arises from the photon recoil associated only with the *spontaneously* emitted photon. This is because the absorbed lattice photon is a σ-polarized standing wave, which gives no recoil (to lowest order) to the atom. Therefore, for highly localized atoms, fluorescence spectroscopy will probe the atoms' vibrational motion only in the direction that the fluorescence photons are detected. This result generalizes to probe spectroscopy, and to lattices of higher dimensionality.

Raman sidebands occur in fluorescence and probe spectra from lattices of any dimension, as illustrated in Figs. 2c, 3c and 9(a)-(d). The atomic motion near the bottom of the potential wells is approximately separable, and the states are products of two or three 1D oscillator states. For the four beam 3D lin⊥lin lattice described in sect. III.B, the optical potential for tightly bound atoms can be approximated by an anisotropic harmonic oscillator with oscillation frequencies $\hbar\omega_{osc,z} = 2\cos\theta_L \sqrt{U_0 E_R}$ and $\hbar\omega_{osc,x} = \hbar\omega_{osc,y} = \sin\theta_L \sqrt{U_0 E_R}$. Only one set of Raman side bands will be observed, centered at the corresponding oscillation frequencies, when photons are detected along these Cartesian axes. Verkerk et al. (1994) report that sidebands corresponding to the

oscillation along directions other than the observation axis are in fact seen in probe spectra; this has been interpreted as a breakdown of the harmonic oscillator model (Grynberg, private communication, 1995). In principle, one can use the amplitude asymmetry of a pair of Raman sidebands in the fluorescence spectrum of higher dimensional lattices to extract the "temperature" of that degree of freedom as discussed in sect. II for the 1D case. However, in 3D lattices the atom density may be sufficiently large that Raman gain/absorption of the spontaneously emitted photons can distort the spectrum thus preventing a measurement of the temperature (Rolston, private communication, 1995).

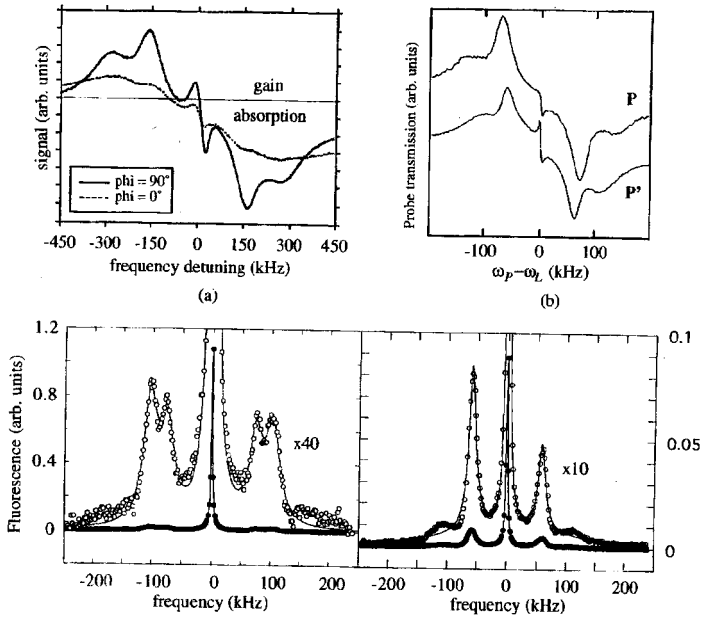

Fig. 9. (a) Probe transmission spectrum from a two-dimensional lattice of the Hänsch type. Solid and dotted lines are data measured for different relative phases of the two standing waves forming the lattice (from Hemmerich and Hänsch (1993), reprinted with permission). (b) Probe transmission spectrum from a three-dimensional lattice of the Grynberg type. Data is shown for different probe propagation directions **P** and **P'** (from Grynberg et al. (1993), reprinted with permission).
(c) Fluorescence spectrum measured with a lattice of the type shown in Fig. 5a. The spectrum is measured along $\hat{\mathbf{x}}+\hat{\mathbf{z}}$, so that two separate oscillation frequencies are observed. (d) Same as (c), but measured along $\hat{\mathbf{x}}$, so that only one oscillation frequency is observed.

Let us finally address the width of the observed Raman sidebands. It can be shown that a harmonic oscillator coupled to the electromagnetic field is characterized solely by the frequency of oscillation and the energy damping rate (Cohen-Tannoudji et al., 1992). For the conditions leading to the spectrum of Fig. 2c with the appropriate Lamb-Dicke

suppression factor, this rate is approximately $2.7\times10^4/s$, which should lead to a sideband width of $\approx 4\,kHz$. The apparent width of the sidebands is nearly ten times larger and indicates that a simple harmonic oscillator model is not sufficient. The Raman sideband width seen in the spectra is in fact almost completely determined by anharmonicity of the optical potential. A perturbation calculation shows that neighboring Raman lines, corresponding to pairs of levels $|n\rangle$, $|n+1\rangle$, are separated by a frequency $E_R/\hbar$. A full band structure calculation confirms that this anharmonic shift indeed accounts for the major frequency deviations from the simple harmonic oscillator model, and both models agree well with the experimentally measured sideband frequency (Jessen et al., 1992).

Hemmerich et al. have measured probe transmission spectra using an intense probe beam (Hemmerich et al., 1994b). In that case the atom/lattice/probe interaction cannot be treated by lowest order perturbation theory, and multiphoton transitions between vibrational states become important. The result is the appearance of sub-harmonics in the spectrum at frequencies ω_{osc}/n, for processes involving n probe photons and n lattice photons. These subharmonics have been seen in probe transmission spectra for n up to 5.

2. The Rayleigh Component

Fluorescence spectra typically contain a coherent component associated with the steady state of the system under study. In 1D and 2D lattices the atomic density in the detection volume decays rapidly due to transverse heating, and it is clear that a steady state does not exist in the strict sense; as a result the coherent component vanishes (Cooper and Ballagh, 1978). Nevertheless, normal modes other than the steady state also contribute to the Rayleigh feature centered at the lattice frequency, but such contributions are broadened according to their finite evolution rates. In the secular regime the Rayleigh line is associated with scattering events that begin and end in the same, or a nearly degenerate quantum state. In spectra from 1D (2D) lattices these contributions may be Doppler broadened due to motion in the unbound dimensions if the direction of measurement is not parallel (coplanar) with the lattice beams. In a deep 3D lattice the atomic density decays much more slowly because there is cooling in all dimensions and an approximate steady state exists on time scales up to a few hundred ms. Furthermore, most atoms occupy states that are tightly bound in all directions and Doppler broadening is negligible. The experimental spectrum of Fig. 9(c) and (d) show a correspondingly narrow Rayleigh line. Indeed the width of the Rayleigh features in fluorescence spectra from 3D lattices has generally been close to the instrumental resolution, in which case it is doubtful that physical information about the lattice dynamics can be extracted.

The Rayleigh feature observed in probe transmission spectra is associated with a similar class of normal modes as the Rayleigh feature in the fluorescence spectra, except that probe

transmission spectra do not contain a contribution from the steady state of the system (Courtois and Grynberg, 1992). For 1D (2D) lattice spectra probed in non-parallel (non-planar) configurations, the dominant contribution to the Rayleigh feature in probe spectroscopy is a so-called "recoil induced resonance" (Courtois et al., 1994; Guo, 1994), which is closely analogous to Doppler broadened Rayleigh scattering in the fluorescence spectrum. Consider the case of a 1D optical lattice, where atoms move freely in the plane perpendicular to the 1D axis. Stimulated Raman transitions then couple pairs of eigenstates that differ only with respect to the transverse atomic momentum. Because the transverse momentum distribution is Maxwell-Boltzmann, there will be a population difference between such states. Raman transitions of the type analogous to those of Fig. 3b occur when $\delta_P = \Delta\mathbf{k}\cdot\mathbf{v}_\perp$, where $\Delta\mathbf{k} = \mathbf{k}_p \pm \mathbf{k}_L$ is the change in photon wave vector due to the scattering event, and $\mathbf{v}_\perp$ is the atom velocity in the transverse plane. The magnitude of the probe gain or absorption is determined by the population difference between the initial and final states and the recoil induced resonance line is therefore the derivative of the Doppler line shape in the fluorescence spectrum. This interpretation is confirmed by a close examination of the central feature of Fig 3c (Courtois et al., 1994).

In deep 3D lattices the majority of atoms occupy tightly bound states and a recoil induced resonance is unlikely to occur. In this situation it is non-trivial to identify the system modes associated with the Rayleigh feature. Experimental 3D probe transmission spectra contain Rayleigh features having widths of a few hundred Hz (Hemmerich et al., 1993) which do not scale with the photon scattering rate as expected based on the master equation, Eq. (13) (Rolston, private communication, 1995). It is presently unresolved what dynamical evolution modes of the atom/lattice system might be responsible for such long time scales and unexpected scaling laws. Courtois and Grynberg (1992) have proposed a mechanism that involves a wave mixing process, in which either the probe beam or one of the lattice beams is scattered off a grating of atomic density or magnetization. Guo (1995a; 1995b) has shown that the observed feature cannot be fully explained in this fashion, and has proposed a mechanism involving a recoiled-induced resonance between quasicontinuum states. Further study is necessary however to establish how the small population in such states might account for the large observed signal.

IV. New Developments

A. Cooling by Adiabatic Expansion in Optical Lattices

A near-resonant optical lattice will localize atoms with a center-of-mass distribution that is much narrower than the separation between potential wells. If the optical lattice is used

primarily as a source of cold atoms, this microscopic atomic localization is of no direct advantage, and it is lost when the lattice beams are extinguished and the atoms released. It is therefore advantageous to trade the atomic localization for a decrease in temperature, e. g. by adiabatic expansion in the optical potential wells. Adiabatic cooling has been demonstrated in an intense, blue-detuned 1D lattice by Chen et al. (1992), and in a 3D lattice of the type shown in Fig. 5 by Kastberg et al. (1995). To illustrate the basic principle we discuss adiabatic expansion for a harmonically bound atom, with a thermal distribution of population characterized by a Boltzmann factor f_B. If the oscillator frequency is decreased, e. g. by lowering the lattice light intensity, the energy separation between vibrational states will decrease. We assume that the change in the oscillator frequency is slow enough to be adiabatic, the condition being that $(d\omega_{osc}/dt)\times(1/\omega_{osc}) << \omega_{osc}$, yet fast enough that dissipative processes can be ignored. In that case the vibrational populations remain unchanged, and the system temperature has obviously been reduced. Because the Boltzmann factor remains unchanged during the expansion we have $f_B = e^{-\hbar\omega_i/k_B T_i} = e^{-\hbar\omega_f/k_B T_f}$, and therefore $T_f = T_i\,\omega_f/\omega_i$, where ω_i, ω_f and T_i, T_f are the initial/final oscillation frequencies and temperatures. For a true harmonic oscillator there is no lower bound on the oscillation frequency, and therefore no lower limit for adiabatic cooling.

In an optical lattice the microscopic potential wells have finite depth, and adiabatic cooling therefore stops when the lattice becomes shallow enough to allow atoms to escape from their original potential wells either by tunneling or above-barrier motion. Kastberg et al. (1995) proposed a simple band theory for adiabatic expansion in a 1-dimensional scalar potential, from which a cooling limit can be derived. In this model, atoms are initially assumed to occupy tightly bound states, and the band structure, Fig. 10a, is well known from the tight binding approximation of solid state physics (Ashcroft and Mermin, 1976). During the adiabatic expansion process this band structure adiabatically evolves into that of free momentum states, Fig. 10b. Thus the final momentum distribution relates in a particularly simple fashion to the initial distribution of population over Bloch states, as illustrated in Fig. 10c. One can then show that the final momentum distribution and temperature depends only on the lattice constant R and the Boltzmann factor f_B that initially characterized the population distribution over bound states. In a 1D lattice one finds

$$\frac{T}{T_R} = \left(\frac{2\pi/R}{k}\right)^2 \frac{1+4f_B+f_B^2}{12(1-f_B)^2} \tag{22}$$

where $k_B T_R/2 = E_R$. This result can be generalized to a cubic 3D lattice, where we again find $T/T_R \propto (2\pi/Rk)^2$. This simple theory was found to be in reasonable quantitative agreement with the experiment of Kastberg et al. (1995).

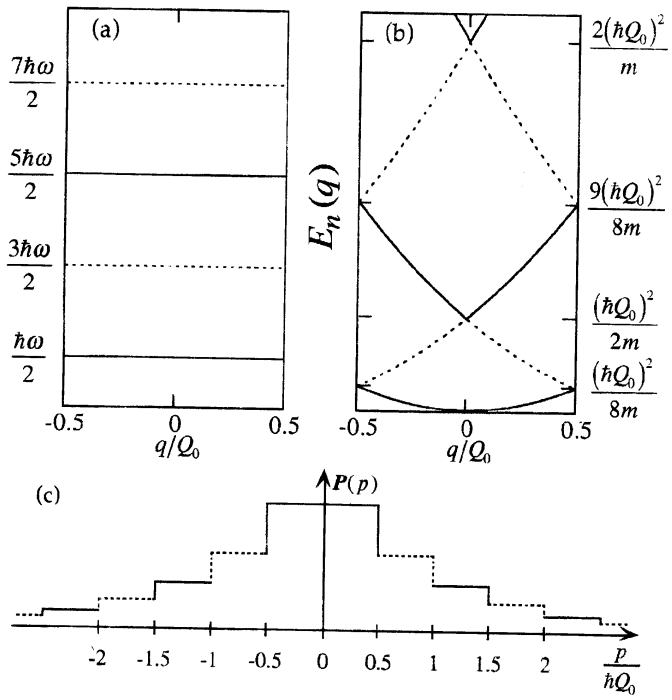

Fig. 10. (a) Band structure in a scalar 1-dimensional lattice potential in the tight binding regime. The lattice constant is $2\pi/Q_0$. (b) Band structure in the same potential, but in the free particle regime. During adiabatic cooling the tight binding Bloch states evolve adiabatically into free particle Bloch states. One can show that, in the tight binding regime, all Bloch states within a band are equally populated; since the adiabatic evolution conserve all populations this is true also for the free particle Bloch states. (c) The corresponding momentum distribution. Solid and dotted lines indicate odd and even numbered bands and their contributions to the final momentum distribution. From Kastberg et al. (1995).

Equation (22) suggests that the adiabatic cooling limit might be improved if atoms are trapped in an optical lattice with a very large lattice constant. Adiabatic cooling in a far-off-resonant lattice configuration with arbitrarily large R in all directions has been demonstrated by (Anderson et al., 1994). However, since a large optical potential well has closely spaced bound states and therefore $f_B \approx 1$, even for atoms that are initially very cold, this approach has so far not been particularly successful. It is possible that Raman sideband cooling (Taïeb et al., 1994) may be used to cool atoms to the vibrational ground state of the lattice. In that case adiabatic release from a lattice of the type shown in Fig. 5

would lead to a temperature as low as $T_R/4$, corresponding to $50\,nK$ in the case of Cs atoms.

B. Bragg Scattering in Optical Lattices

The experiments discussed to in sects. II and V have investigated the localization, and quantized motion of atoms in optical lattices. As the lattice light field is a topologically stable configuration, the atoms are trapped at strictly periodic positions, and therefore the density distribution possesses long-range correlations. Optical lattices studied so far have been only sparsely populated; for a 3D lattice of the type shown in Fig. 5 an atom density of 10^{11} cm^{-3} corresponds to a filling fraction of only f~0.01. Even so, long-range order has important consequences for the propagation of light through the atomic sample. In particular, waves scattered into well defined directions other than forward will be phase-matched, i. e. the atomic order will give rise to Bragg reflection. Two factors make this Bragg scattering process markedly different from Bragg scattering in solid crystals. First, the optical lattice constant is of order 1 µm, compared to a few Å in solids, and Bragg scattering therefore occurs at optical rather than x-ray wavelengths. Second, we consider scattering of a weak probe beam tuned near an atomic resonance, where the absorption cross section is enhanced and the atomic response is highly dispersive.

Atoms arranged in a lattice described by reciprocal lattice vectors $\{\mathbf{K}\}$ will Bragg reflect a probe with wave vector $\mathbf{k}_p$ into the direction $\mathbf{k}_p + \mathbf{K}$ when one satisfies the Bragg condition, $2\mathbf{k}_p \cdot \mathbf{K} = -K^2$, written here in the von Laue form. As shown in sect. III, the set of vectors $\{\mathbf{K}_j\}$ are given by differences between the lattice beams wave vectors $\{\mathbf{k}_i\}$. Bragg reflection therefore occurs for a probe beam propagating parallel to a lattice beam,$\{\pm\mathbf{k}_i\}$, into directions parallel to the remaining beams $\{\pm\mathbf{k}_{j\,i}\}$.

A Bragg reflection experiment was performed by G. Birkl et al. (1995) on Cs atoms in a three dimensional optical lattice (Fig 5). In that work, atoms were first allowed to equilibrate and become spatially ordered. The lattice light field was then quickly extinguished, and a weak probe beam, tuned close to the atomic transition used to form the lattice, was applied along one of the directions for which Bragg reflection occurs. Performing the experiment in the absence of the lattice laser beams avoids a contribution from nearly degenerate four-wave mixing; however, once the lattice potential is removed the center-of-mass distribution of the initially localized atoms starts expanding ballistically. By measuring the temporal dependence of the Bragg reflected signal one gains information on the atomic localization and temperature. Weidemüller (1995) have used an alternative approach, in which a probe resonant with a separate transition of much shorter wavelength was Bragg reflected in the presence of the lattice light field. In this situation the large

frequency difference between lattice and probe beams prevents any contribution from four-wave mixing.

Physical information about the trapped atoms is available in the reflected intensity. In the following we ignore diffraction effects, and assume that the atom density is so low that multiple reflections can be ignored. Consider then an atomic sample distributed over n infinite planes, illuminated by a plane probe wave. The Bragg reflection coefficient for intensity is

$$R_n = n^2 R\ f_n(\theta_P, \Delta_P), \tag{23}$$

where R is the single plane reflectivity and $n^2 R$ is the familiar Bragg result. One can show that $n^2 R \sim \beta (N\sigma(\Delta_p))^2$,where N is the number density of atoms in the lattices, $\sigma(\Delta_p)$ is the absorption cross section, and Δ_P the detuning of the probe from atomic resonance. The parameter $\beta = \exp\left\{-(2\pi\Delta x / d)^2\right\}$ is known as the Debye-Waller factor. In this expression d is the separation between lattice planes, and Δx is the RMS width of the atomic center-of-mass distribution perpendicular to the lattice planes. The factor $f_n(\theta_P, \Delta_P)$ in Eq. (23) accounts for loss and dispersion.

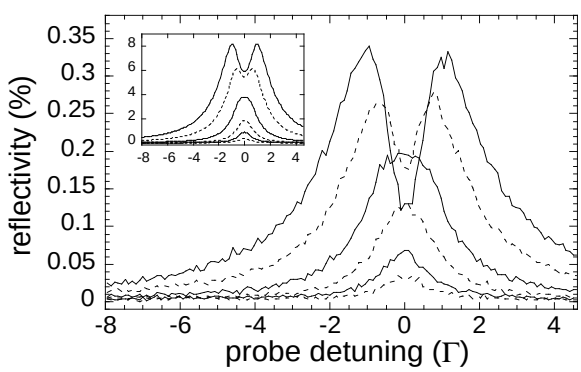

Fig. 11. Bragg reflectivity as a function of probe laser detuning. Atomic densities in the lattice range from 3×10^9 to 8×10^{10} cm^{-3}, increasing by roughly a factor of 2 between traces. The inset shows calculated spectra for the same parameters. (from Birkl et al., 1995).

Fig. 11 shows the measured Bragg reflection intensity as function of probe detuning, for various atomic densities. At low density the reflection lineshape is a Lorentzian with the natural linewidth Γ. As atomic density is increased the lineshape is broadened, and

eventually develops a dip near resonance. This behavior is easily interpreted in terms of optical density of the atomic sample. At low density the sample is optical thin and the reflection spectrum is similar to a disordered vapor, but enhanced by a factor ~10^5. As the atom density is increased both probe and reflected waves are attenuated, and the effective number of planes contributing to the Bragg scattering is reduced. The effect is most pronounced near resonance where the optical density is maximum, and eventually a dip will develop. A calculation of the lineshape using the foregoing model of Bragg reflection (insert of Fig. 11) is in qualitative agreement with the experimental spectra. When the lattice light is extinguished, the atomic center-of-mass distribution expands ballistically and the Bragg reflectivity decays. The atom temperature can therefore be extracted from the time-dependent Debye-Waller factor. These measurements of atom temperature and localization are in reasonable agreement with measurements based on spectroscopy or time-of-flight measurements of the atomic momentum distribution.

Bragg reflection is a new tool which complements the spectroscopic techniques discussed in section 5. The strong dependence of Bragg reflectivity on atomic localization provides a unique probe of both equilibrium dynamics and driven atomic motion. One can also measure the change in the lattice constant with lattice detuning and atomic density (Birkl et al., 1995) due to the back-action of the atomic polarizability on standing wave light fields (Deutsch et al. 1995).

C. OUTLOOK

Most studies of optical lattices have so far been aimed at understanding the basic process of laser cooling and trapping, as well as the physics involved in fluorescence and probe spectroscopy. These efforts have been largely successful, and it appears likely that the main focus of both theory and experiment will shift in the near future. One area of considerable practical importance is the application of optical lattices to the control of atomic motion. Examples range from the use of optical lattices in preparing cold atomic samples for atomic fountain clocks, to the development of new lithographic techniques based on light controlled deposition of atoms onto substrates.

To illustrate the potential of light controlled atom deposition, consider that in the 1D optical lattice experiments discussed in sect. II, Rb atoms were found to be localized in optical potential wells with an RMS center-of-mass spread of $\lambda/15$, corresponding to a FWHM of 100 nm (Jessen et al., 1992). If such atoms could be deposited on a surface they would form lines with a resolution well below the current state-of-the-art of optical lithography. In a practical version of this experiment, Timp et al. (1992) used a 1D optical lattice to control the deposition of a Na atomic beam on a surface. Atoms were first laser

cooled in the direction transverse to the beam, and then channeled along planes defined by an optical lattice oriented parallel to the atomic beam axis. Immediately downstream from the lattice the atoms struck a substrate, where they formed a regular array of lines a few tens of nm wide. McClelland et al. (1993) have demonstrated similar deposition schemes using 1D and 2D lattices and chromium atoms. The combination of nm resolution and the ability to deposit, in parallel, features over a very large area, makes atom lithography appear an attractive technology; much development still remains however, before it can be demonstrated that light controlled deposition of arbitrary nano-scale patterns is feasible.

One of the most interesting aspects of optical lattices is the close analogy between the motion of cold atoms in the periodic optical potential and systems in condensed matter physics. The flexibility with which we can modify the parameters of an optical lattice makes this an attractive model system for studying fundamental problems, e. g. transport in a periodic system. Such studies are crucial for the microscopic understanding of electrical and thermal conductivity in solids, and increasingly they are relevant to studies of biophysical processes such as energy transport in photosynthesis. Though the optical lattice is far removed from the highly complex systems of condensed matter, and thus no direct information can be inferred, its relative simplicity opens the door to well controlled experiments that can be precisely modeled. In addition, cooperative phenomena may be studied in a realizable system which has long been an idealized "toy" model for condensed matter physicists - the dilute, weakly interacting gas. Preliminary studies of the effects of dipole-dipole interaction between atoms in a 3D lattice have been carried out by Goldstein et al. (1996). Practical realization of these model systems requires two important experimental advances: trapping atoms in the lattice in an essentially dissipation free environment, and increased atomic densities.

The typical near-resonant optical lattice is not particularly well suited for such work both because it is highly dissipative and because inelastic long range dipole-dipole interactions between atoms in the lattice, along with other types of light assisted collisions, tend to limit the atomic density. The rate of dissipative processes, such as spontaneous emission and inelastic collisions, are proportional to the excited state population, and it is therefore apparent that the design of new types of lattices that minimize atomic excitation is of considerable interest. To this end Grynberg et al. have proposed a "gray" optical lattice such that atoms are trapped near points where they are in a "dark state" (Grynberg and Courtois, 1994), and such that they only couple weakly to the field away from these equilibrium points. A similar, closely related lattice has been demonstrated experimentally by Hemmerich et al. (1995).

Another approach towards reducing the excited state population is to continue to trap atoms at points where they strongly couple to the field, but to increase both the lattice light

detuning Δ, and intensity I_L. In that regime the photon scattering rate is $\gamma_s \propto I_L/\Delta^2$ whereas the potential well depth is $U_0 \propto I_L/\Delta$, so that dissipation can be made arbitrarily small while still maintaining deep wells in the optical lattice. One difficulty associated with these lattices is that the very absence of dissipation makes it difficult to load atoms into the optical potential wells. This problem is much more severe than for the "gray" lattices discussed above, in which bound states are efficiently populated by a combination of Sisyphus cooling and velocity selective coherent population trapping (Aspect et al., 1989). In a far-off-resonance lattice, loading may be achieved through a separate laser-cooling field, or perhaps through the adiabatic transfer of population from an initial near-resonance lattice.

Once atom trapping in a dissipation free lattice is accomplished, it may be possible to implement new cooling mechanisms to improve the atomic localization, or to generate specific quantum states of the atomic center-of-mass motion. Raman sideband cooling might for example be implemented in a far-off-resonance lattice, in a manner analogous to that of trapped ions (Heinzen and Wineland, 1990). Theoretical studies by Taïeb et al. (1994) indicate that this method might allow one to cool atoms to the vibrational ground state of their individual potential wells. If this can indeed be accomplished, then such atoms might be used as a starting point for adiabatic cooling to sub-recoil temperatures, or for experiments with driven atomic motion. As an example, parametric driving of an atom initially in the vibrational ground state will produce an oscillating atomic wave packet which is squeezed alternately in position and momentum space (Marksteiner et al., 1995).

One of the most basic physical phenomena characterizing quantum motion is tunneling. Tunneling dynamics are expected to become important if the rate of dissipation in an optical lattice can be reduced sufficiently. In that case, an optical lattice may constitute an attractive and flexible model system in which to study the propagation of matter waves in periodic potentials. One of the most striking manifestations of tunneling in a periodic lattice is the existence of "Bloch oscillations" (Wannier, 1962) of the atomic momentum under the influence of a constant force. The observation of such oscillations in a crystal lattice is greatly complicated by strong interactions and extremely rapid decoherence of the electronic motion, and thus it has been accomplished only in semiconductor superlattice structures (Mendez and Bastard, 1993). An optical lattice constitutes a new system in which a conceptually simpler version of this physical phenomenon may be studied, i. e. noninteracting particles in a simple lattice, free of dissipation, and with an external force applied through a constant accelleration of the lattice in the laboratory frame. Very recently, experiments have seen Bloch oscillations directly in the time domain (Dahan et al., 1996) and performed spectroscopy of the "Wannier-Stark ladder" (Wilkinson et al., 1996). These developments illustrate how optical lattices offer a new "laboratory" in which one

can study a wide variety of phenomena that combine concepts from atomic, optical, and condensed matter physics.

Acknowledgments

The authors thank S. L. Rolston for helpful discussions. This work was supported in part by the National Science Foundation Contract No. PHY-9503259.

References

Anderson, B. P., Gustavson, T. L., and Kasevich, M. (1994). *Proc. International Quantum Electronics Conference*, QPD2-1/3, May 8-13, Anaheim California.

Ashcroft, N. W. and Mermin, N. D., (1976). *Solid Sate Physics*. Holt-Saunders, Philadelphia.

Aspect, A., Arimondo, E., Kaiser, R., Vansteenkiste, N., Cohen-Tannoudji, C. (1989). Journ. Opt. Soc. Am. B **6**, 2112.

Berg-Sørensen, K. (1994). Phys. Rev. A **49**, R4297.

Berg-Sørensen, K., Castin, Y., Mølmer, K., and Dalibard, J. (1993). Europhys. Lett. **22**, 663.

Birkl, G., Gatzke, M., Deutsch, I. H., Rolston, S. L., and Phillips, W. D. (1995). Phys. Rev. Lett. **75**, 2823.

Carmichael, H. J. (1993). *An Open Systems Approach to Quantum Optics*. Springer Berlin.

Castin, Y., Dalibard, J., and Cohen-Tannoudji, C. (1991). In *Light Induced Kinetic Effects on Atoms, Ions, and Molecules* , p.5 (L. Moi, S. Gozzi, C. Gabbanini, E. Arimondo, and F. Strumia eds.). ETS Editrice PISA.

Castin, Y. and Dalibard, J. (1991). Europhys. Lett. **14**, 761.

Castin, Y. (1992). Ph. D. dissertation, Ecole Normale Supérieure, Université Paris VI.

Castin, Y., Berg-Sørensen, K., Dalibard, J., and Mølmer, K. (1994). Phys. Rev. A **50**, 5092.

Castin, Y. and Mølmer, K. (1995). Phys. Rev. Lett. **74**, 3772.

Chen J., Story, J. G., Tollet, J. J., and Hulet, R. G. (1992). Phys. Rev. Lett. **69**, 1344.

Cohen-Tannoudji, C. (1991). In *Les Houches, Session LIII, Fundamental Systems in Quantum Optics* (J. Dalibard, J. M Raimond, and J. Zinn-Justin

eds.). Elsevier Science Publisher.

Cohen-Tannoudji, C., Dupont-Roc, J., and Grynberg, G. (1992). *Atom-Photon Interactions* pp. 326-329, 384-386, 427-436. Wiley-Interscience, New York.

Cooper, J. and Ballagh, R. J. (1978). Phys. Rev. A **18**, 1302.

Courtois, J.-Y. and Grynberg, G. (1992). Phys. Rev. A. **46**, 7060.

Courtois, J.-Y (1993). Ph. D. dissertation, Ecole Polytechnique, Paris.

Coutois, J.-Y., Grynberg., G., Lounis, B., and Verkerk, P. (1994). Phys. Rev. Lett. **72**, 3017.

Dahan, M. B., Peik, E., Reichel, J., Casyin, Y., and Salamon, C. (1996). Phys. Rev. Lett. **76**, 4508.

Dalibard, J. and Cohen-Tannoudji, C. (1989). Journ. Opt. Soc. Am. B **6**, 2023.

Deutsch, I. H., Spreeuw, R. J. C., Rolston, S. L., and Phillips, W. D. (1995). Phys. Rev. A **52**, 1394.

Diedrich, F., Bergquist, J. C., Itano, W. M. and Wineland, D. J. (1989). Phys. Rev. Lett. **62**, 403.

Doery, M., Widmer, M., Bellanca, J., Vredenbregt, E., Bergeman, and Metcalf, H. (1994). Phys. Rev. Lett. **72**, 2546.

Gardiner, C. W., Parkins, A. S., Zoller, P. (1992). Phys. Rev. A **46**, 4363.

Gisin, N. and Percival, I. C. (1992). J. Phys. A **25**, 5677.

Goldstein, E. V., Pax, P., and Meystre, P (1996). Phys. Rev. A **53**, 2604 (1996).

Grison, D., Lounis, B., Salomon, C., Courtois, J.-Y. and Grynberg, G. (1991). Europhys. Lett. **15**, 149.

Grynberg, G., Lounis, B., Verkerk, P., Courtois, J.-Y., and Salomon, C. (1993). Phys. Rev. Lett. **70**, 2249.

Grynberg, G. and Courtois, J.-Y. (1994). Europhys. Lett. **27**, 41.

Guo, J. (1994). Phys. Rev. A. **49**, 3934.

Guo, J. (1995a). Phys. Rev. A. **51**, 2338.

Guo, J. (1995b). Phys. Rev. A. **52**, 1458.

Gupta, R., Padua, S., Bergeman, T., and Metcalf, H. (1992). In *Laser Manipulation of Atoms and Ions*, p. 345 , (W. D. Phillips, E. Arimondo and F. Strumia, eds.) North Holland, Amsterdam.

Hänsch, T. and Schawlow, A. (1975). Opt. Com. **13**, 68.

Heinzen, D. J. and Wineland, D. J. (1990). Phys. Rev. A **42**, 2977.

Hemmerich A. and Hänsch T. W. (1993). Phys. Rev. Lett. **70**, 410.

Hemmerich, A., Zimmermann, C., and Hänsch, T. (1993). Europhys. Lett. **22**, 89.

Hemmerich, A., Weidemüller, M., and Hänsch, T. (1994a). Europhys. Lett. **27**,

427.
Hemmerich, A., Zimmermann, C., and Hänsch, T. W. (1994b). Phys. Rev. Lett. **72**, 625.
Hemmerich, A., Weidemüller, M., Esslinger, T., Zimmermann, C., and Hänsch, T. W. (1995). Phys. Rev. Lett. **75**, 37.
Holland, M., Marksteiner, S., Marte, P., and Zoller, P. (1996). Phys. Rev. Lett., **76**, 3683.

Jessen, P. S., Gerz, C., Lett, P. D., Phillips, W. D., Rolston, S. L., Spreeuw, R. J. C., and Westbrook, C. I. (1992). Phys. Rev. Lett. **69**, 49.
Jessen, P. S. (1993). Ph. D. dissertation, University of Aarhus, Århus.
Jurczak, C., Sengstock, K., Kaiser, R., Vansteenkiste, N., Westbrook, C. I., Aspect, A. (1995). Opt. Comm. **115**, 480.
Kastberg, A., Phillips, W. D., Rolston, S. L., Spreeuw, R. J. C., and Jessen, P. S. (1995). Phys. Rev. Lett. **74**, 1542.
Lett, P. D., Watts, R. N., Westbrook, C. I. , Phillips, W. D., Gould, P. L. and Metcalf, H. J. (1988). Phys. Rev. Lett. **61**, 169.
Lounis, B., Verkerk, P., Courtois, J.-Y., Salomon, C., and Grynberg, G. (1993). Europhys. Lett. **21**, 13.
Marksteiner, S., Ellinger, K., and Zoller, P. (1996). Phys. Rev. A, **53**, 3409.
Marksteiner, S., Walser, R., Marte, P. and Zoller, P. (1995). Appl. Phys. B **60**, 145.
Marte, P., Dum, R., Taïeb, R., and Zoller, P. (1993a). Phys. Rev. A. **47**, 1378.
Marte, P., Dum, R., Taïeb, R., Lett, P. D. and Zoller, P. (1993b). Phys. Rev. Lett. **71**, 1335.
McClelland, J. J., Scholten, R. E., Palm, E. C., and Celotta, R. J. (1993). Science **262**, 887.
Mendez, E. E. and Bastard, G. (1993). Phys. Today **46**, 34.
Mølmer, K., Castin, Y., and Dalibard, J. (1993). Journ. Opt. Soc. B **10**, 524.
Petsas K. I., Coates, A. B., and Grynberg, G. (1994) Phys. Rev. A **50**, 5173.
Salomon, C., Dalibard, J., Phillips, W. D., Clairon, A. and Guellati, S. (1990). Europhys. Lett. **12**, 683.
Tabosa, J. W. R., Chen, G., Hu, Z., Lee, R. B. and Kimble, H. J. (1991). Phys. Rev. Lett. **66**, 3245.
Taïeb, R., Dum, R., Cirac, J. I., Marte, P., and Zoller, P. (1994). Phys. Rev. A. **49**, 4876.
Timp, G., Behringer, R. E., Tennant, D. M., Cunningham, J. E., Prentiss, M.,

and Berggren, K. K. (1992). Phys. Rev. Lett. **69**, 1636.

Ungar, P. J., Weiss, D. S., Riis, E. and Chu, S. (1989). Journ. Opt. Soc. Am. B **6**, 2058.

Verkerk, P., Lounis, B., Salomon, C., Cohen-Tannoudji, C., Courtois, J.-Y., and Grynberg, G. (1992). Phys. Rev. Lett. **68** , 3861.

Verkerk P., Meacher, D. R., Coates, C. B., Courtois, J.-Y., Guibal, S., Lounis, B., Salomon, C. and Grynberg, G., (1994). Europhys. Lett. **26**, 171.

Wannier, G. H. (1962). Rev. Mod. Phys. **34**, 645.

Weidemüller, M., Hemmerich, A., Gorlitz, A., Esslinger, T., and Hänsch, T. W. (1995). Phys. Rev. Lett. **75**, 4583.

Weiss, D. S., Riis, E., Shevy, Y., Ungar, P. J. and Chu, S. (1989). Journ. Opt. Soc. Am. B **6**, 2072.

Westbrook, C. I., Watts, R. N., Tanner, C. E., Rolston, S. L., Phillips, W. D. and Lett, P. D. (1990). Phys. Rev. Lett. **65**, 33.

Wilkinson, S. R., Bharucha, C. F., Madison, K. W., Niu, Q., and Raizen, M. G. (1996). Phys. Rev. Lett **76**, 4512.

Wineland, D. and Dehmelt, H. (1975). Bull. Am. Phys. Soc. **20**, 637.

Wineland, D. J. and Itano, W. M. (1979) Phys. Rev. A **20**, 1521.